Journal of Sound and Vibration 330 (2011) 721–742

Contents lists available at ScienceDirect

Journal of Sound and Vibration

journal homepage: www.elsevier.com/locate/jsvi

Cracked beam identification by numerically analysing the nonlinear behaviour of the harmonically forced response

Ugo Andreaus *, Paolo Baragatti

Sapienza Università di Roma, Dipartimento di Ingegneria strutturale e geotecnica, Via Eudossiana 18, 00184 Roma, Italy

ARTICLE INFO

Article history:
Received 7 June 2009
Received in revised form
26 April 2010
Accepted 25 August 2010
Handling Editor: I. Trendafilova

ABSTRACT

Numerical evaluation of the flexural forced vibration of a cantilever beam having a transverse surface crack extending uniformly along the width of the beam was performed to relate the nonlinear resonances to the crack presence, location, and depth. To this end, the qualitative characteristics, namely phase portrait distortions, sub- and super-harmonic components in the Fourier spectrum, and curved shape of the modal line were considered. Furthermore, quantitative parameters, such as the eccentricity and the excursion of the orbit, and the harmonic amplitude in the spectrum were measured. Then, an identification procedure was proposed which was based on the intersection of constructed surfaces which allowed to identify the structural damage. The acceleration record of the beam tip was sufficient to detect the existence of the crack and to identify crack depth and site.

1. Introduction

The presence of a crack could not only cause a local variation in the stiffness, but it could affect the mechanical behaviour of the entire structure to a considerable extent. For these reasons, there is a need to understand the dynamics of cracked structures. The vibration characteristics of cracked structures can in fact be useful for an on-line detection of cracks (non-destructive testing) without actually dismantling the structure [1]. Therefore, the development of structural integrity monitoring techniques is received increasing attention in recent years. Among these monitoring techniques, it is believed that the monitoring of the global dynamics of a structure offers favourable alternative if the on-line (in service) damage detection is necessary. In order to identify structural damage for vibration monitoring, the study of the changes of the structural dynamic behaviour due to cracks is required for developing the detection criterion [2].

Among the techniques employed for crack detection are vibration-based methods, which offer an effective and fast means of detecting fatigue cracks in structures [3].

Most of the techniques are based on vibration measurement and analysis because, in most cases, vibration based methods can offer an effective and convenient way to detect fatigue cracks in structures. Generally, vibration based methods can be classified into two categories [4]: the linear approach and the nonlinear approach. By linear approaches the presences of cracks in a target object are detected through the monitoring of changes in resonant frequencies [5] or in damping factors [6] or in mode shapes [7]. However, some researches have shown the linear detection procedures do not always come up to practical requirement because of low sensitivity to defects [8].

* Corresponding author. Tel.: +390644585297; fax: +39064884852.
E-mail addresses: ugo.andreaus@uniroma1.it (U. Andreaus), paolo.baragatti@uniroma1.it (P. Baragatti).

0022-460X/$ - see front matter © 2010 Elsevier Ltd. All rights reserved.
doi:10.1016/j.jsv.2010.08.032

Nomenclature

a	crack depth
A	area of the cross-section
b	distance of the spring from the built-in end of the beam
B	bending stiffness of the intact beam
C	shear stiffness of the intact beam
$d_{\max}^{\mathrm{dam}}$	maximum displacement of the damaged system
$d_{\min}^{\mathrm{dam}}$	minimum displacement of the damaged system
$d_{\max}$	maximum displacement of the system
$d_{\min}$	minimum displacement of the system
D	total excursion on the displacement axis
D_v	variation of the total excursion on the displacement axis
e_d	the eccentricity of the orbit with respect to the origin on the displacement axis in the phase portrait
E	Young's modulus
f_c	first natural frequency of the beam when the crack is closed
f_o	first natural frequency of the beam when the crack is open
f_b	first bilinear natural frequency of the beam when the crack is breathing
f_F	frequency of the driving force
F	intensity of the driving force
G	shear rigidity of the material
h	height of the cross-section
h_r	relative amount of magnitude of super- or sub-harmonic components with respect to the amplitude of the fundamental component
H_f	amplitude of the fundamental component
H_s	magnitude of super- or sub-harmonic components
I	indicator of efficiency in damage detection
I_x	inertia moment of the cross-section with respect to the x-axis
J	indicator of comparison among structural models
k_c	stiffness of the bilinear spring when the crack is closed
k_o	stiffness of the bilinear spring when the crack is open
L	beam length
m	mass of the equivalent single-degree-of-freedom oscillator
m_b	mass of the equivalent single-degree-of-freedom oscillator when the crack is breathing
m_c	mass of the equivalent single-degree-of-freedom oscillator when the crack is closed
m_o	mass of the equivalent single-degree-of-freedom oscillator when the crack is open
n	order of the harmonic component
n_h	number of harmonic components
n_p	number of crack positions
n_s	number of crack severities
n_Ψ	number of damage parameters
p	non-dimensional position of the crack along the z-axis
s	crack severity
T_c	first natural period of the beam when the crack is closed
T_o	first natural period of the beam when the crack is open
T_b	first bilinear natural period of the beam when the crack is breathing
w	width of the cross-section
x, y, z	spatial coordinates
δ_c	deflection of the beam tip loaded by a statically applied force with the same amplitude of the sinusoidal excitation when the crack is closed
δ_o	deflection of the beam tip loaded by a statically applied force with the same amplitude of the sinusoidal excitation when the crack is open
η	ratio between driving and bilinear frequencies
ν	Poisson's ratio
ρ	mass density of the beam
χ	shear factor of the cross-section
$\boldsymbol{\Psi}$	set of the damage parameters
Ψ	list of the values of the damage parameters
Ψ	value of a single damage parameter
ω_c	circular frequency of the equivalent single-degree-of-freedom oscillator when the crack is open
ω_o	circular frequency of the equivalent single-degree-of-freedom oscillator when the crack is closed

There are two main categories of crack models used in the methods: open crack models and breathing crack models. Most researchers have assumed that the crack in a structural member is open and remains open during vibration. This assumption was made to avoid the complexity resulting from nonlinear behaviour when a breathing crack is presented. Nevertheless, during vibration, a crack will open and close due to an externally applied loading. During the vibration of a structure, edges of the crack come into and out of contact, leading to sudden changes in the dynamic response of the structure. This phenomenon is known as the breathing process of the crack. By introducing the concept of a breathing crack, an intensive investigation can reveal small changes in the dynamic response of the cracked element. These changes in dynamic response can be useful for detection of cracks [9].

Chondros et al. [10] evidenced that using an open crack model assumption to interpret vibration measurements for a fatigue breathing crack will lead to incorrect conclusions, in particular one would presume that the crack severity is smaller than what it really is. Only a few papers were devoted to the detection of actual fatigue cracks, due perhaps to the difficulty to generate a true fatigue crack and to the technical simplicity to carve a slot. Andreaus and Baragatti [11]

addressed the initiation and propagation of fatigue cracks in metallic beams and their influence on the free-vibration dynamic response; even if that was a "linear" method, it seemed to be able to account for and to detect the presence of the so-called "breathing" crack. These features opened the door to future developments towards nonlinear detection methods.

Nonlinear effects make the response of beams with a fatigue breathing crack more difficult to predict than that of a notched beam. However, on the other hand, their presence accentuates the difference of the damaged dynamics from the undamaged one. Then, if a vibration measure which is sensitive to presence of nonlinear behaviour is selected, the identification of a fatigue crack, which is more likely to appear on real structure, is more easy to achieve than that of an always open crack [12].

When a cracked object is subjected to a single harmonic input, main distinctive features of such a vibration system are the appearance of nonlinear characteristics in the dynamic response, such as nonlinear distortions of time-histories, super-harmonic components, and sub-harmonic resonances. In summary, the nonlinear effect analysis based methods would be much more sensitive to presences of cracks than the linear vibration based methods. Thus, increasingly over recent years, attentions have been focused on the investigations of the nonlinear effects caused by the presence of breathing cracks and associated applications to the problem of damage detection.

The papers [2,13–18] present methods for analysis of steady-state vibration of a beam with breathing cracks, which open and close during vibration. Some useful conclusions for diagnosing cracked beams systems are proposed in [19]. An approach has been proposed in [4] for nonlinearity detection in vibrating systems with multiple degrees of freedom, which is based on the concept of nonlinear output frequency response functions; it requires testing on inspected systems twice with the applied input forces differing in strength in the two tests. The approach determines the position of the nonlinear component in an mdof system directly from the applied input forces and the corresponding responses of the masses in the system.

From the above literature review it is observed that the models used for breathing cracks are either one-dimensional continuous or discrete models or bilinear single degree of freedom or two- or multi-degree of freedom systems. In the close vicinity of the crack, the stress and displacement field is three-dimensional. Therefore, the existing models cannot accurately simulate the beam near the crack. To accurately model the three-dimensional stress and displacement fields near the breathing crack, a contact model with three-dimensional finite element needs to be used. However, if the whole beam is modelled, using three-dimensional finite elements the computational effort is high. As a compromise, a contact model for a breathing crack with two-dimensional finite elements is proposed herein. The proposed model can be extended to three-dimensional models of cracked structures.

The objective of the work presented in [20] is to study the relative amplitudes of the harmonics as their positions vary along the frequency axis when the exciting frequency is changed, in a bi-dimensional model of a cantilever beam with root crack. This study is useful for the detection of cracks in beams in the sense that it demonstrates that the response spectrum may be more sensitive to the presence of cracks for some excitation frequencies.

The proposed approaches therefore have potential in the fault diagnosis of mdof systems and structures, but they are limited only to the detection of the presence of damage.

Detection of fatigue cracks in flexible bars by the super-resonant vibration method proposed in [21,22] may be carried out by estimating the size of the fatigue crack by the value of the spectral ratio between the second or the third and fundamental harmonics, using a preliminary constructed calibration curve.

The main idea of the procedure proposed in [23,24] for crack location and size estimation is based on the determination of the vibration response nonlinearity around the second superharmonic and the one-half subharmonic resonances at different parameters of driving force. Moreover, the abrupt change of the nonlinearity of vibration response when driving force is applied close to the crack indicates its location. In such a way the procedure of damage detection allows to estimate both the crack size and location in beams.

The paper proposed herein is a novel method inasmuch it is a fully identification procedure allowing to qualitatively detect the presence of damage and quantitatively determine the extension and the position of a fatigue crack; moreover, the bi-dimensional model of the cantilever beam accounts for contact and detachment of the crack interfaces. Damage indicators physically related to the nonlinear features of the forced response under harmonic excitation are introduced, namely the ratios between the second and third superharmonic and one-half subharmonic components with respect to the fundamental one, the eccentricity of the orbit with respect to the origin on the displacement axis of the phase portrait, the variation of the total excursion of the damaged system with respect to the total excursion of the intact system on the displacement axis of the phase portrait. Using preliminary constructed calibration surfaces permits to simultaneously evaluate crack size and location by solving a system of two quadratic equations; the reliability of these results can be checked by comparing them with those one obtained by another independent system. Even very small cracks can be identified due to the significant magnitude of the signal distortions involved. Moreover, the driving force may be applied not necessarily near the (presumably unknown) position of the crack, and only one acceleration measure is needed in any position along the beam.

The purpose of the present paper was to develop the analytical approach enabling the simulation of vibration of a beam with a closing edge transverse crack in order to solve direct (determination of dynamic characteristics of a beam at given crack parameters) and inverse (estimation of crack parameters by the known values of corresponding dynamic characteristics) problems of damage diagnostics. The distortions of the orbits in the phase plane and the relative amplitudes of the harmonics, as their positions varied along the frequency axis when the exciting frequency is changed,

were chosen as the dynamic characteristics to be investigated. The efficiency of the proposed method was verified by a numerical example of a cracked beam under cantilever boundary conditions. Three different numerical models were considered for discussion in this paper. The first one is a two-dimensional finite element model, which was developed as a reference model. The second model was a ten-element or equivalently 20-dof cantilevered beam that had the same dimensions and material properties of first model. Lastly, an equivalent single-dof spring-mass-damper system was considered for comparison; in fact, at low frequencies the beam structure can be modelled as a single-degree-of-freedom piece-wise linear system which has different stiffnesses during stretching and compression of the crack.

In the forward problem, the sinusoidal harmonic force was applied on the free end of the beam and harmonic response was obtained on the force application point; the changes in harmonic responses corresponding to the change in crack depth and location were evaluated for crack detection analysis. The inverse problem was also solved. To estimate the position and size of the crack, a simple relation was establish, which related the so-called Nonlinear Damage Indicators (NDIs), namely excursion and eccentricity of the orbit in the phase portrait and the amplitude of the super- or sub-harmonics, to the location and depth of the crack. The estimated NDIs increased with crack distance (from the beam tip) and depth following a four-order polynomial law and therefore the NDIs were used as indicators for crack place and size evaluation. These results were fitted into a surface in a least squares sense. Both the crack size and position were predicted from the NDIs recorded numerically by a virtual accelerometer.

2. System models

2.1. Generalities

This problem physically represents a straight beam of length L which contains one single-side edge fatigue crack of depth a and has a rectangular uniform cross-section of height h and width w, Fig. 1; the cantilever beam is clamped at the left end and free at the right end. The crack is located at the upper edge of the beam at a distance d from the fixed end and $p=d/L$ is the dimensionless crack position; the severity $s=a/h$ of the crack is expressed in terms of the ratio between the depth to the height of the cross-section. Linear isotropic stress–strain material properties are assumed.

A cracked cantilever beam of length $L=0.3$ m and cross-section $w\times h=0.02\times 0.02$ m^2 was tested and studied by Rizos et al. [25]; the material is mild steel having Young's modulus $E=206.8$ GPa, Poisson's ratio $\nu=0.3$, and mass density $\rho=7850$ kg/m^3. The vibration frequencies and mode shapes of the beam containing an edge crack of various sizes at different positions along the beam were obtained by Kam and Lee [26] from either experiments [25] or finite element analyses of the cracked beam when experimental data were not available. In the case of the finite element analyses of the cracked beam, the stiffness matrix of the cracked element proposed by Qian et al. [27] was used to generate the required data for crack identification.

With the ever increasing sophistication of available equipment more effective models had to be built to better interpret the experimental results. As far as monodimensional continuous models are concerned, two approaches are considered, namely continuous and local flexibility. In the continuous flexibility scheme, differential equation and the boundary conditions are derived for the cracked beam via variational principles [28,2,29]. In particular, the modification of the stress field induced by the crack is incorporated through a local empirical function which assumes an exponential decay with the distance from the crack, and includes parameters that had to be evaluated by experiments or using the displacement field in the vicinity of the crack found with fracture mechanics methods (stress intensity factors). In the local flexibility models [30,31,25,15,10,32], the main idea in modelling the crack is to introduce a local compliance matrix, connecting longitudinal, bending and shear forces and displacements near the crack tip; the elements of the local flexibility matrix describe the reduced stiffness due to the crack by means of the stress intensity factors [33]. Alternatively, the cracked beam can be discretized via the Finite Element Method by using both 1-D [34,27,35] and 2-D elements [36,37,16,20]. In addition, the nonlinear behaviour of a beam with a closing crack vibrating in its lowest modes of vibration can be simulated through multi-degree-of-freedom models with bilinear stiffnesses [36,37,38,15,39].

The mechanical behaviour of an opening crack is different from that of a closing crack. To analyse these behaviours in fracture mechanics when general time-varying loads are applied is a very complex problem; in fact the stress–strain field

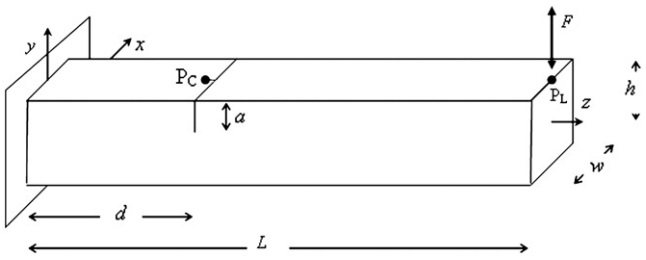

Fig. 1. Cantilever beam with a single-edge crack.

at the crack tip, the form of the crack interface and the level of the crack's opening and closing are all required [27]. Thus, the equations of motion are nonlinear and non-smooth, and, definitively, there is no exact solution of these equations. Consequently, a numerical method [30,37,16] must be adopted.

While the beam is vibrating, the state of the crack section varies from detachment to compression, i.e. the crack opens and closes with time. This results in a modification of the crack section stiffness, the extremal values being the stiffness of the open crack and that of the intact beam. Thus, the nonlinear behaviour of the closing crack introduces the characteristics of the nonlinear systems. However, for many practical applications, the system can be considered bilinear, and the fatigue crack can be introduced in the form of the so-called "breathing crack" model which opens when the normal strain near the crack tip is positive, otherwise it closes [40]. Distinction should be made between the first natural frequencies $f_c=1/T_c$ and $f_o=1/T_o$, of the two constituent sub-models (the subscripts "c" and "o" mean "closed crack" and "open crack", respectively) and the first natural frequency f_b of the system, the so-called bilinear frequency [13]:

$$f_b = \frac{2}{T_c+T_o} = 2\frac{f_c f_o}{f_c+f_o} \tag{1}$$

where T_c and T_o are the natural periods of the two sub-models. Eq. (1) strictly holds for a single-degree-of-freedom oscillator with a bilinear stiffness; as it will be seen in Section 3.1, Eq. (1) approximates with good accuracy the first frequency of the beam with breathing crack.

In this paper, for comparison's sake, the data of Rizos et al. [25] were adopted, and a consistent mass matrix was used in the dynamical analysis with implicit time integration, provided that the Newmark method and full Newton iteration were used.

2.2. Two-dimensional finite element model

Herein, the plane-stress elastodynamic response of an edge cracked panel was studied; static and transient dynamic analyses were performed using a proprietary finite element package ADINA 8.5 [41]. A 2-D solid (plane stress) nine-node iso-parametric element was chosen to discretize the body and the finite element mesh consisted of 380 elements and 1627 nodes. Two-dimensional contact surfaces were specified to model planar contact behaviour between solid elements at the crack interfaces [42].

The deflections $\delta_o<0$, $\delta_c>0$ of the beam tip loaded by a statically applied force with the same amplitude of the sinusoidal excitation were calculated; in the first case the force downloads to open the crack, whereas in the second case it uploads to close the crack, Fig. 1.

2.3. Contact modelling

Contact surfaces are defined as surfaces that are initially in contact or are anticipated to come into contact during the response solution. Two-dimensional contact surfaces are formed of a series of linear contact segments and each segment is bounded by two nodes, Fig. 2. A distinction should be made within these two surfaces between the contactor surface and the target surface, in as much, in the converged solution, the target nodes can overlap the contactor body and not vice-versa; in other words, according to the contact condition, the contactor nodes cannot be inside the target body, but the

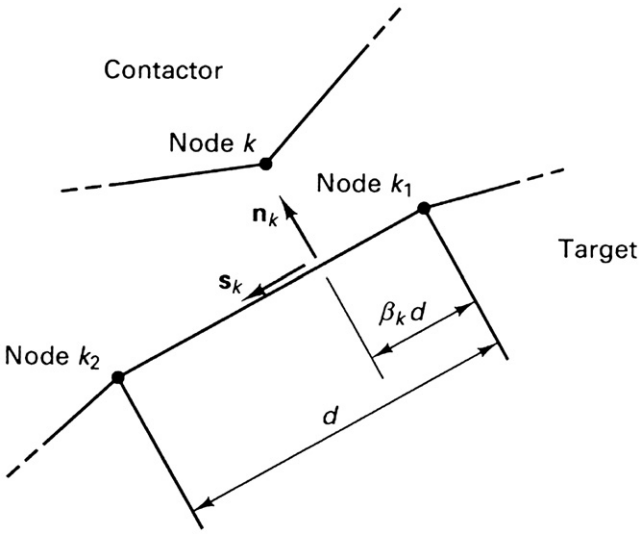

Fig. 2. Two-dimensional case of contact.

target nodes can be inside or outside the contactor body. A node of the contactor surface can come into contact with a segment of the target surface.

In frictionless contact, the possible states of the contactor nodes and/or segments are as follows: (i) the gap between the contactor node and target segment is open (no contact); (ii) formerly closed gap has opened; a tensile force onto the contactor node is not possible (tension release); and (iii) the gap between the contactor node and the target segment is closed; a compression force is acting onto the contactor node.

The finite element approach is used to discretize the governing continuum mechanics equations and the contact conditions (Fig. 3). To exemplify the formulation of the governing finite element equations, let us consider the two-dimensional case of contactor and target bodies shown schematically in Fig. 2, where the target segment corresponding to contactor node k is defined by nodes k_1 and k_2. The target point k_t is the closest point of the target segment k_1-k_2 to the contactor node k. By assembling for all contactor nodes the nodal point force vectors, the discretization of the continuum mechanics equations corresponding to the conditions at time $t+\Delta t$ gives [41]

$$\mathbf{f}_i(\mathbf{u}) = \mathbf{f}_e - \mathbf{f}_c(\mathbf{u},\boldsymbol{\lambda}) \tag{2a}$$

$$\mathbf{c}_c(\mathbf{u},\mathbf{l}) = \mathbf{0} \tag{2b}$$

where $\mathbf{u}$, $\boldsymbol{\lambda}$ are the solution variables, namely the nodal point displacements $\mathbf{u}$ and the normal traction components $\boldsymbol{\lambda}$; $\mathbf{f}_i$ is the vector of internal nodal forces equivalent to element stresses; $\mathbf{f}_e$ is the vector of applied external nodal forces; $\mathbf{f}_c$ is the nodal force vector, which is obtained by assembling for all contactor nodes the nodal point force vectors due to contact; $\mathbf{c}_c$ is the vector of contact conditions the components of which are as many as the contactor nodes.

The incremental finite element equations of motion including contact conditions for solution of Eq. (2) are obtained by linearization about the last calculated state at time t:

$$\begin{bmatrix} (\mathbf{K}_T+\mathbf{K}_{uu}^c) & \mathbf{K}_{u\lambda}^c \\ \mathbf{K}_{\lambda u}^c & \mathbf{K}_{\lambda\lambda}^c \end{bmatrix} \begin{Bmatrix} \Delta\mathbf{u} \\ \Delta\boldsymbol{\lambda} \end{Bmatrix} = \begin{Bmatrix} \mathbf{f}_e^{t+\Delta t} - \mathbf{f}_i - \mathbf{f}_c \\ -\mathbf{c}_c \end{Bmatrix} \tag{3}$$

where $\Delta\mathbf{u}$ and $\Delta\boldsymbol{\lambda}$ are the increments in the solution variables $\mathbf{u}$ and $\boldsymbol{\lambda}$, $\mathbf{K}_T$ is the usual tangent stiffness matrix including geometric nonlinearities, not including contact conditions; $\mathbf{K}_{uu}^c$,$\mathbf{K}_{u\lambda}^c$,$\mathbf{K}_{\lambda u}^c$,$\mathbf{K}_{\lambda\lambda}^c$ are the contact stiffness matrices. It is worth to be noticed that the vector $\mathbf{f}_e$ is evaluated at current time $t+\Delta t$, while the other matrices and vectors are evaluated at the previous time t.

In order to simplify the notation, the following relations are understood to refer to any contactor node k. Using the definition of the "gap function" g, that is the (signed) distance from the node k to the target point k_t, the conditions for normal contact can be stated as the Signorini's conditions for displacement [43]:

$$g \geq 0 \tag{4a}$$

$$\lambda \geq 0 \tag{4b}$$

$$g\lambda = 0 \tag{4c}$$

Note that the contact force and gap function are of course expressed in terms of the nodal displacements.

Eq. (4) can be interpreted by considering the following cases:

(1) *No contact*: if $g>0$, the equality in Eq. (4c) implies $\lambda=0$; when there is no contact, all contact tractions must be zero. Fig. 3.
(2) *Sticking contact*: if $\lambda>0$, the equality in Eq. (4c) implies $g=0$.

Accordingly, any component of the vector $\mathbf{c}_c$ which refers to any contactor node k can be written as

$$c_{cw} = \hat{w}(g,\lambda) \tag{5}$$

and the following constraint function can be used [41]:

$$\hat{w}(g,\lambda) = \frac{g+\lambda}{2} - \sqrt{\left(\frac{g-\lambda}{2}\right)^2 + \varepsilon_N} \tag{6}$$

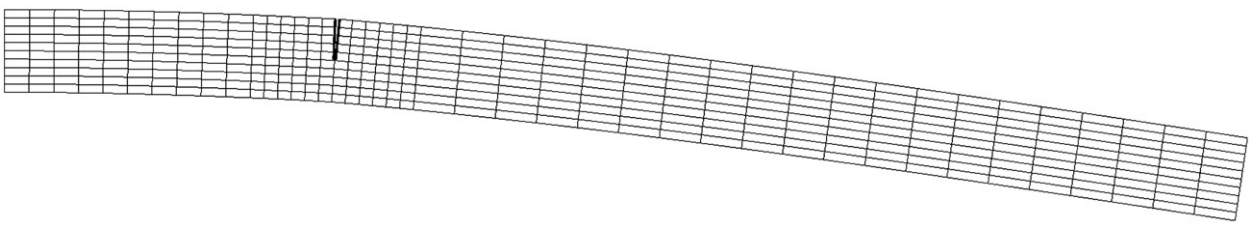

Fig. 3. Finite element mesh of the 2-D model.

where ε_N is very small but larger than zero. Eq. (6) defines a suitable function of g and λ such that the solutions of $\hat{w}(g,\lambda)=0$ satisfy conditions (4) within a reasonable accuracy.

2.4. Solution of nonlinear equations of motion

The solution of the nonlinear dynamic response of the finite element system at hand is obtained using the incremental formulation presented in Section 2.3, an iterative solution procedure and a time integration algorithm. For notation's conciseness, the following symbols are introduced:

$$\mathbf{U}=\left\{\begin{array}{c}\mathbf{u}\\ \boldsymbol{\lambda}\end{array}\right\},\quad \mathbf{F}=\left\{\begin{array}{c}\mathbf{f}_e\\ \mathbf{0}\end{array}\right\},\quad \mathbf{R}=\left\{\begin{array}{c}\mathbf{f}_i+\mathbf{f}_c\\ \mathbf{c}_c\end{array}\right\},\quad \mathbf{K}=\left[\begin{array}{cc}(\mathbf{K}_T+\mathbf{K}^c_{uu}) & \mathbf{K}^c_{u\lambda}\\ \mathbf{K}^c_{\lambda u} & \mathbf{K}^c_{\lambda\lambda}\end{array}\right]$$

The solution of the equilibrium at time $t+\Delta t$ requires an iteration procedure: by linearizing the response of the finite element system about the conditions at time $t+\Delta t$, iteration $(i-1)$, the following equations are obtained:

$$\Delta\mathbf{F}^{(i-1)}=\mathbf{F}_{t+\Delta t}-\mathbf{R}^{(i-1)}_{t+\Delta t} \tag{7a}$$

$$\mathbf{K}^{(i-1)}_{t+\Delta t}\,\Delta\mathbf{U}^{(i)}=\Delta\mathbf{F}^{(i-1)} \tag{7b}$$

$$\mathbf{U}^{(i)}_{t+\Delta t}=\mathbf{U}^{(i-1)}_{t+\Delta t}+\Delta\mathbf{U}^{(i)} \tag{7c}$$

In each iteration an out-of-balance load vector is calculated, Eq. (7a); an increment in displacements is given by Eq. (7b), and the iteration proceeds until the out-of-balance load vector $\Delta\mathbf{F}^{(i-1)}$ or the displacement increments $\Delta\mathbf{U}^{(i)}$ are sufficiently small.

Newmark's method with $\delta=1/2$ and $\alpha=1/4$ is used for time integration and the robustness of the numerical procedure has been checked in all the performed analyses.

2.5. Beam finite element model

The study has been performed using a finite element model of the beam (Fig. 4), in which a so-called closing crack model, fully open or fully closed, is used to represent the damaged cross-section; the model was validated against experimental results of free vibrations [11]. Intact parts of the beam are modelled by Timoshenko-type finite elements with two nodes and 2 dofs (transverse displacement and rotation) at each node. To relate the crack length to a local flexibility parameter, the crack was modelled by a bilinear rotational spring, Fig. 5, of constants k_c and k_o in the vicinity $z=b$ of the cracked cross-section, Fig. 4; $k_c=EI_x$ is the stiffness of the beam when the crack is closed. The stiffness k_o when the crack is open can be identified by equating the tip deflection of the Timoshenko-type beam with reduced local flexibility

$$\delta_o=\left[\left(\frac{L^3}{3B}+\frac{L}{C}\right)+\frac{b^2}{k_o}\right]F \tag{8}$$

to the y-displacement of point load of the 2-D FEM model, denoted P_L in Figs. 1 and 4; the parameters $B=EI_x$ and $C=\chi GA$ are, respectively, the bending and the shear stiffness of the beam, whereas $A=wh=2\times10^{-4}$ m^2, $I_x=wh^3/12=2^4\times10^{-8}/12$ m^4, and $\chi=5/6$ are, respectively, the moment of inertia with respect to the x-axis, the area, and the shear factor of the uncracked cross-section; E and G are, respectively, Young's and Lamè's modulus of the material. The beam of Fig. 4 is then discretized into 15 elements and 17 nodes.

2.6. Single-degree-of-freedom model

As already observed, one can qualitatively see that the global stiffness of the cracked beam depends on whether the crack is open or closed. Moreover, due to boundary conditions, loading type and crack location the first mode of the cracked beam's response is primarily involved, that can be reasonably studied by a simple system with bilinear stiffness.

The system consists of a lumped mass m which makes contact with the linear spring k_o when $x<0$ and with the linear spring $k_c>k_o$ when $x>0$. The equations of motion for the system are

$$m\ddot{x}+k_{\mathrm{i}}x=0,\ \mathrm{i}=\mathrm{o}\quad \text{for } x<0\quad \text{and}\quad i=c\quad \text{for } x>0 \tag{9}$$

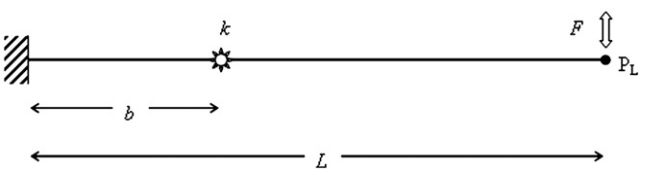

Fig. 4. 1-D beam model.

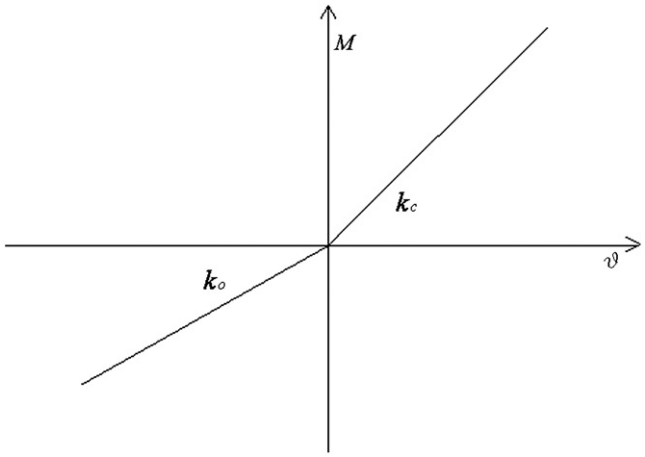

Fig. 5. Bilinear rotational spring.

where the dot indicates differentiation with respect to time. The effective natural frequency f_b of this bilinear single degree-of-freedom system (bsdof) is given by Eq. (1).

Stiffnesses and mass of the bsdof can be identified on the basis of, respectively, compliance and frequency characteristics of the 2-D FEM model:

$$k_i = F/\delta_i, \quad \omega_i = 2\pi f_i, \quad m_i = k_i/(\omega_i)^2, \quad i = c,o \tag{10a}$$

$$m_b \cong (m_c + m_o)/2 \tag{10b}$$

2.7. Suitability of the simpler models

The spring constants of the bilinear rotational spring in the simpler 1-D model of beam can be identified without construction of the 2D FE model. In fact, the spring constant in the closing phase is the elastic rigidity EI_x of the intact beam in simple bending, according to the elementary beam theory, and it is not to be necessarily identified on the basis of the 2-D model. On the other hand, the spring constant K_R in the opening phase is given in terms of the crack length by the expression in [44], derived from the linear fracture mechanics:

$$K_R = \frac{wh^2E}{72\pi\, s^2(0.6384 - 1.036s + 3.7201s^2 - 5.1773s^3 + 7.553s^4 - 7.332s^5 + 2.4909s^6)}$$

It leads to the same results obtained by the identification based on the 2-D model, which was used in this paper only for sample'sake; thus, this simpler model can exist independently without construction of the 2D FE model. As far as the equivalent sdof model is concerned, it can be identified on the basis of the 2-D FE model or of the independent 1-D beam model; in any case, the interest and usefulness for the reduced models of structural dynamic systems is perceived in the literature. The procedure of tuning the parameters of a reduced model, which could be obtained from any full-order model, allow the studying of more complex scenarios at a fairly low computational costs. In fact, once that the spring constants have been easily identified for assigned crack size and position, other parameters, e.g. position, frequency and intensity of the point load, load type and distribution, etc., may be changed and their effects explored in detail.

3. Harmonically forced response

3.1. Generalities

The following non-dimensional parameters were found to be significant: (i) the severity of the crack $s=a/h$ depth-to-height ratio, (ii) the position of the crack $p=d/L$ distance-to-length ratio, and the excitation-to-system frequency ratio, $\eta=f_F/f_b$, where f_F is the frequency of the harmonic excitation and f_b is the first natural frequency of the system.

The dynamic response of the beam depends on the above listed parameters. Detailed features of the response were studied for a damage scenario characterized by the following values of the fundamental parameters: severity factor $s=0.1$, 0.3, and 0.5, position factor $p=0.083$, 0.267, and 0.467, and driven frequency $\eta=1/3$, 1/2, and 2.

For these damages, free vibration of the 2-D FEM model of the cracked beam after impulsive excitation were numerically analysed under instantaneous loading. An impulsive force was transversally applied for a very short while at the tip P_L (Fig. 1) of the closed crack, open crack, and breathing crack beams; then, the frequency content of the y-displacement time-history of the loaded point has been determined via spectral analysis in order to evaluate the lowest

natural frequencies of the beams [42], Table 1. The numerical results were validated against the experimental ones [25,26,11]. It is worth to be noted that the predicted values f_b for the breathing crack beams coincides with those ones given by Eq. (1).

Then the forced vibration of the damaged beam with breathing crack was investigated by applying a 100 N sinusoidal load at the beam tip. The time step was taken about (1/60) times the time-period $T_b=1/f_b$ i.e. 0.0001 s. The Discrete Fourier Transform (DFT) was used to perform spectral analysis of the dynamic response.

3.2. Nonlinear characteristics of the response due to the breathing crack

For each position and severity of the crack, and for each frequency of the driving force, the following results both in time and frequency domains were determined and analysed with reference to the y-motion of the load point P_L (Fig. 1):

- phase portrait in the displacement–velocity domain (Figs. 6a–11a),
- fourier spectrum of the acceleration ($\eta=1/3$, $1/2$) and displacement ($\eta=2$) time-histories (Figs. 6b–11b), and

Table 1
Natural frequencies (Hz) of the 2-D FEM model.

Position	Severity	f_c (Hz)	f_o (Hz)	f_b (Hz)
0.083	0.1	183.3	182.0	182.4
	0.3	183.3	172.5	177.9
	0.5	183.3	143.3	160.0
0.267	0.1	183.3	182.7	182.9
	0.3	183.3	177.0	178.5
	0.5	183.3	160.0	170.0
0.467	0.1	183.3	183.1	183.2
	0.3	183.3	180.0	182.0
	0.5	183.3	173.3	176.7

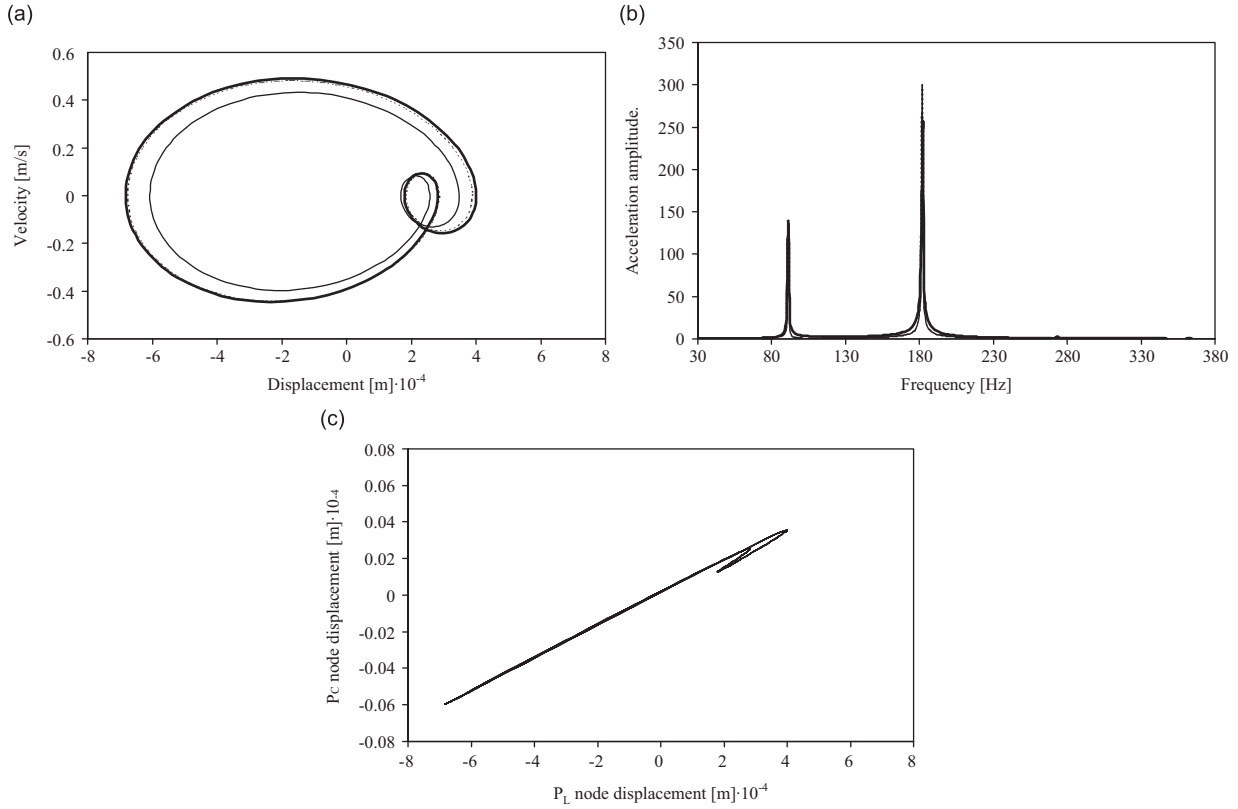

Fig. 6. Case $p=0.08$, $s=0.1$, $\eta=1/2$ (2-D, thick solid line; 1-D, thin solid line; sdof, dashed line): (a) phase portraits, (b) Fourier spectra, and (c) 2-D modal line.

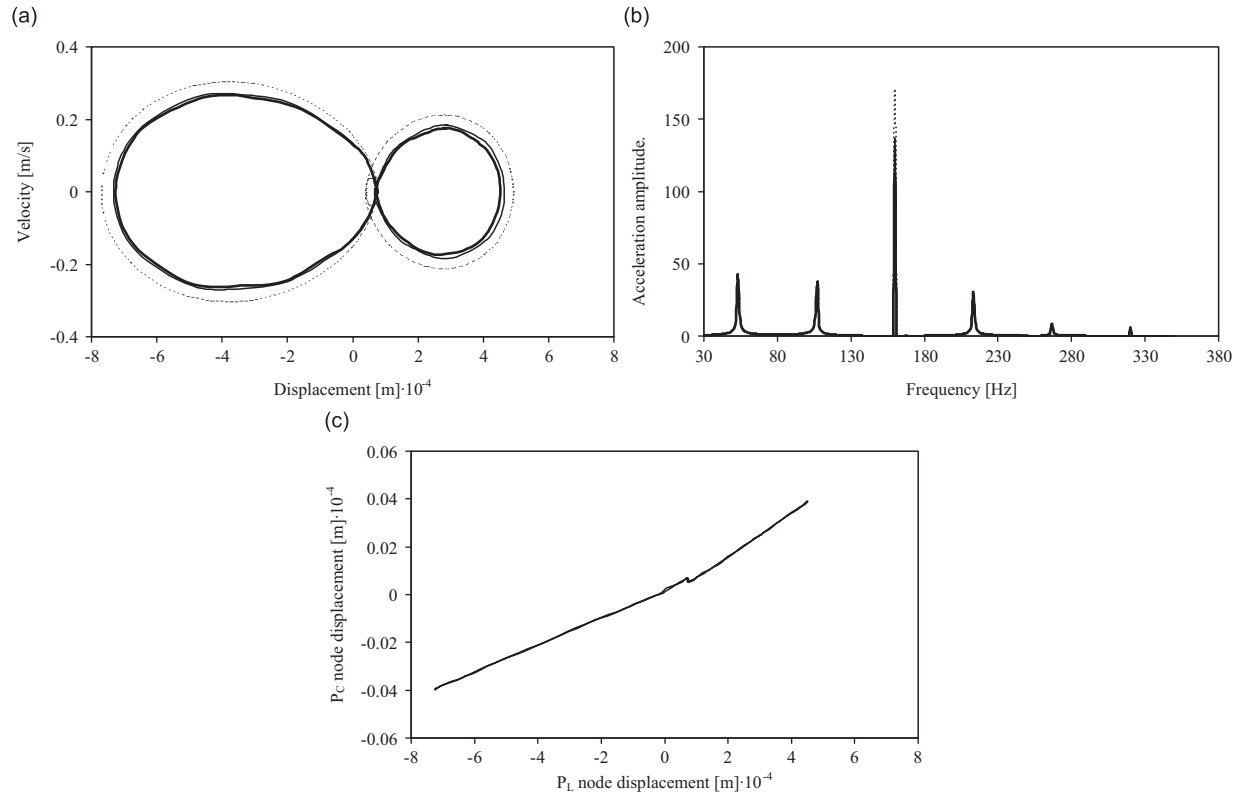

Fig. 7. Case $p=0.08$, $s=0.5$, $\eta=1/3$ (2-D, thick solid line; 1-D, thin solid line; sdof, dashed line): (a) phase portraits, (b) Fourier spectra, and (c) 2-D modal line.

- displacement of point P_C (point near the crack) vs. displacement of point P_L (tip point), Fig. 1, the so-called modal line (Figs. 6c–11c).

For brevity's sake, due to space limits, only selected cases were reported and commented in this section, in order to highlight the main nonlinear features of the dynamic response which can be used to detect the presence of damage, as done in Section 4; the chosen plots allowed to compare the relative performances of the 2-D, 1-D, and sdof models. Different cases have been presented and discussed by one of the authors and his co-workers in [45] by using different tools like Poincaré map and bifurcation diagram.

The phase portraits revealed the appearance of strongly nonlinear phenomena: the relevant plots presented evident distortions, wiggles and recesses. The origin centred ellipse representing the forced response of the undamaged system transformed into curves characterized by circumvolutions or corner points. The phase portrait distortion is in fact one of the strongly nonlinear dynamic characteristics of the cracked systems, which was assumed as a first qualitative Nonlinear Damage Indicator (NDI).

In particular, for the sets of values $p=0.083$, $s=0.5$, $\eta=1/3$ (Fig. 7a), and $p=0.467$, $s=0.5$, $\eta=1/3$ (Fig. 11a), the phase plane portrait was characterized by a "figure-of-eight" shape; a typical diagram is depicted in Fig. 12a which shows the difference (dashed line) between the displacement time-history of the damaged beam (thick line) with respect to that of the intact one (thin line), during one driven period; the dashed line represents the contribution of the prevailing super-harmonic component to the dynamic response. The particular diagram refers to the case $p=0.083$, $s=0.5$, $\eta=1/3$, to the third harmonic component, and to the 2-D solid model, but it is representative of a more general behaviour which can be observed in all the examined cases.

For the sets of values $p=0.083$, $s=0.1$, $\eta=1/2$ (Fig. 6a), $p=0.267$, $s=0.3$, $\eta=2$ (Fig. 8a), $p=0.267$, s=0.5, $\eta=1/2$ (Fig. 9a), and $p=0.467$, $s=0.3$, $\eta=1/2$. (Fig. 10a), a wiggle appears in the phase portrait due to rebounding of the contact surfaces during the closure phase of the crack. Also in this case $p=0.267$, $s=0.5$, $\eta=1/2$, the difference (dashed line) between the displacement time-history of the damaged beam (thick line) with respect to that of the intact one (thin line), during one driven period, is shown (Fig. 12b).

Also the spectral analyses highlighted the high nonlinearity of the response: for the system resonance the harmonic components with the largest magnitude occurred at the natural bilinear frequency f_b, Eq. (1), namely super-harmonics 3

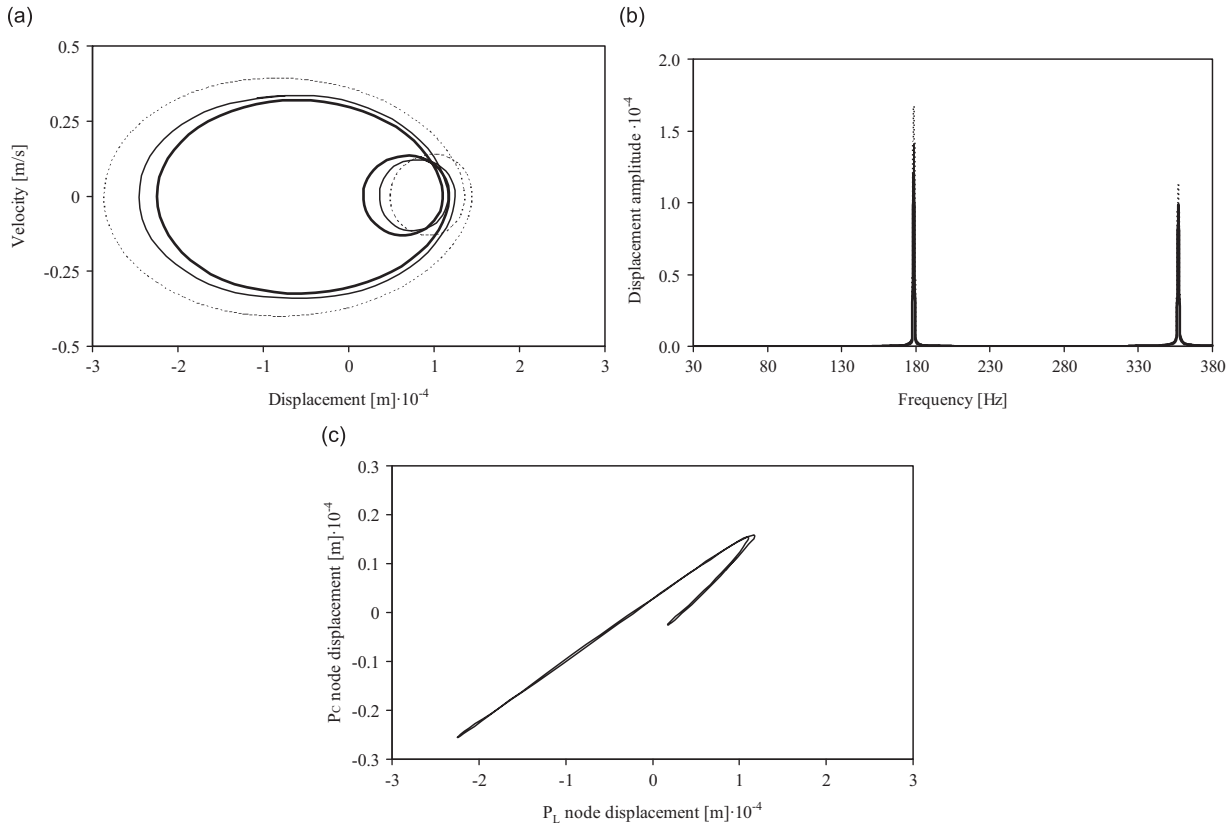

Fig. 8. Case p=0.27, s=0.3, η=2 (2-D, thick solid line; 1-D, thin solid line; sdof, dashed line): (a) phase portraits, (b) Fourier spectra, and (c) 2- D modal line.

(odd) for η=1/3 and 2 (even) for η=1/2, and sub-harmonic 1/2 for η=2. It is obviously noted that an undamaged beam is characterized by linear behaviour (in regime of small displacements and deformations) and therefore exhibits the unique harmonic component at the forcing frequency f_F in the steady-state response, while the harmonic component at the natural frequency is absent.

Furthermore, for $f_F \ll \mathrm{Min}(f_c, f_o)$, other minor components were exactly $f_b + n\, f_F$ ($n = \pm 1, \pm 2, \ldots$) away from the major component at f_b, as already predicted by Chu and Shen [13] limited to the case of response analysis of bilinear single-degree-of-freedom systems.

Thus, the sub- and super-resonances in the FFT spectra (unlike the single harmonic component of the undamaged case) was assumed as a second qualitative NDI. This aspect was observed in Figs. 6b–11b, as far as both the super-harmonic (Figs. 6b, 7b, 9b, 10b, 11b), and the sub-harmonic components (Fig. 8b) were concerned.

Even the modal lines of Figs. 6c–11c emphasized the nonlinear characteristics of the system response: indeed they showed a curved shape and possibly exhibited an offset with respect to the origin. It is by the way reminded that the modal lines of the undamaged system are rectilinear and pass through the origin. The nonlinear trend of the modal lines of the cracked system was therefore assumed as a further (third) qualitative NDI, and noted in the Figs. 6c–11c, even if it was more or less evident.

To sum up the above outlined observations, the presence of a breathing crack introduces nonlinear phenomena into the system. They were evident in the phase portrait, in the FFT spectrum and even in the modal line. Their characteristics can be represented by the so-called qualitative NDIs, namely:

- phase portrait distortions;
- sub- and super-harmonic components in the FFT spectrum; and
- curved shape of the modal line.

These indicators summarise the description of the nonlinear dynamics of the system and introduce to the damage and identification procedure.

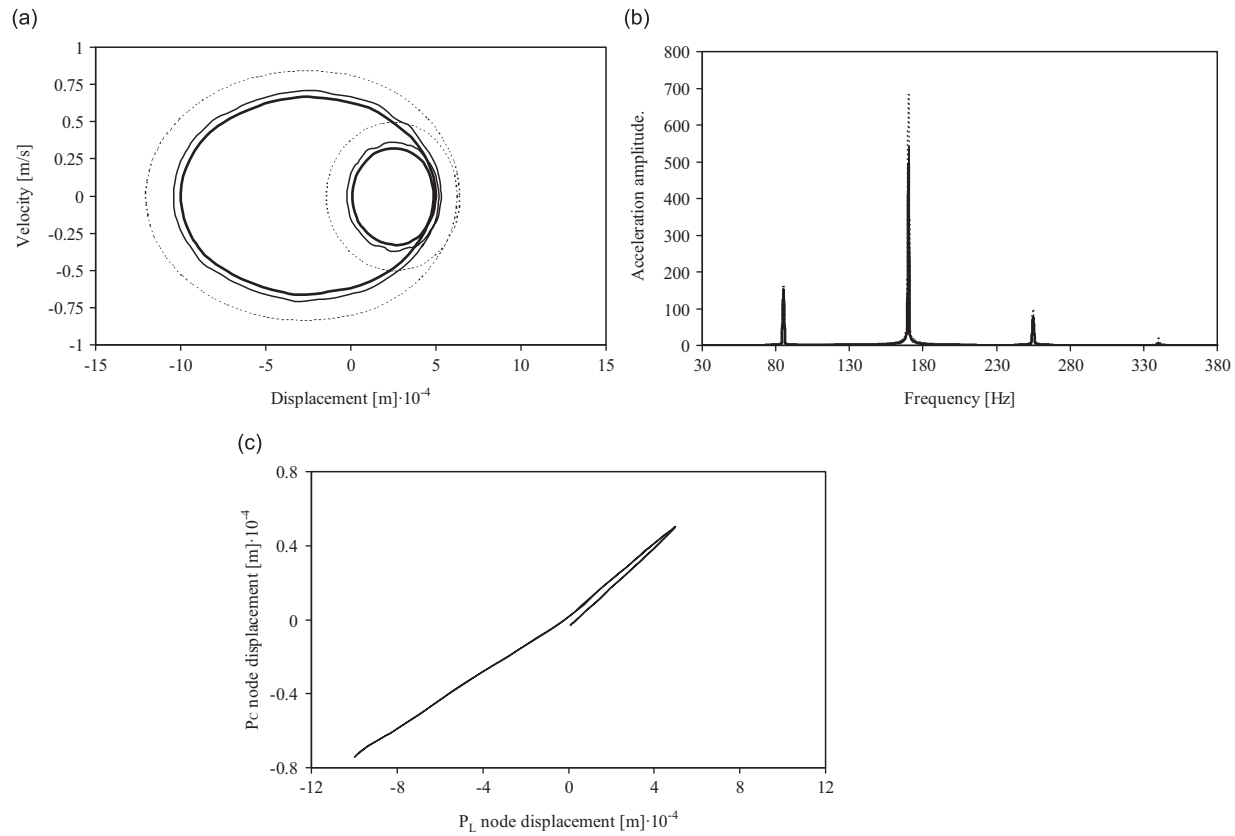

Fig. 9. Case $p=0.27$, $s=0.5$, $\eta=1/2$ (2-D, thick solid line; 1-D, thin solid line; sdof, dashed line): (a) phase portraits, (b) Fourier spectra, and (c) 2-D modal line.

4. Detection of the damage

In order to actually detect the crack presence, the nonlinear phenomena which were described in Section 3.2 and represented by the qualitative NDIs have to be precisely estimated. This is the reason why three quantitative NDIs (Ψ) should be defined.

With reference to the sample phase portrait shown in Fig. 13, the deviation of the damaged system's behaviour from the linear one is denounced by the eccentricity e_d of the orbit with respect to the origin on the displacement axis:

$$e_d = \frac{d_{\max}^{\mathrm{dam}} - d_{\min}^{\mathrm{dam}}}{2} \tag{11}$$

where $d_{\max}^{\mathrm{dam}}$ and $d_{\min}^{\mathrm{dam}}$ are, respectively, the maximum and minimum displacements of the damaged system.

Moreover, defining the total excursion on the displacement axis as, Fig. 13,

$$D = d_{\max} - d_{\min},$$

the variation:

$$D_v = D^{\mathrm{dam}} - D^{\mathrm{int}} \tag{12}$$

of the total excursion D^{dam} of the damaged system with respect to the total excursion D^{int} of the intact system can give another useful measure of the defective state.

Furthermore, as far as the frequency content of the damaged system response in the Fourier spectrum is concerned (Figs. 6b–11b), the existence of $n=1/\eta=3$, 2, 1/2 multiple (super-harmonic) or sub-multiple (sub-harmonic) components of magnitude H_s and their relative amount

$$h_r = \frac{H_s}{H_f} \tag{13}$$

with respect to the amplitude H_f of the fundamental component $n=1$ denounces also presence and intensity of damage.

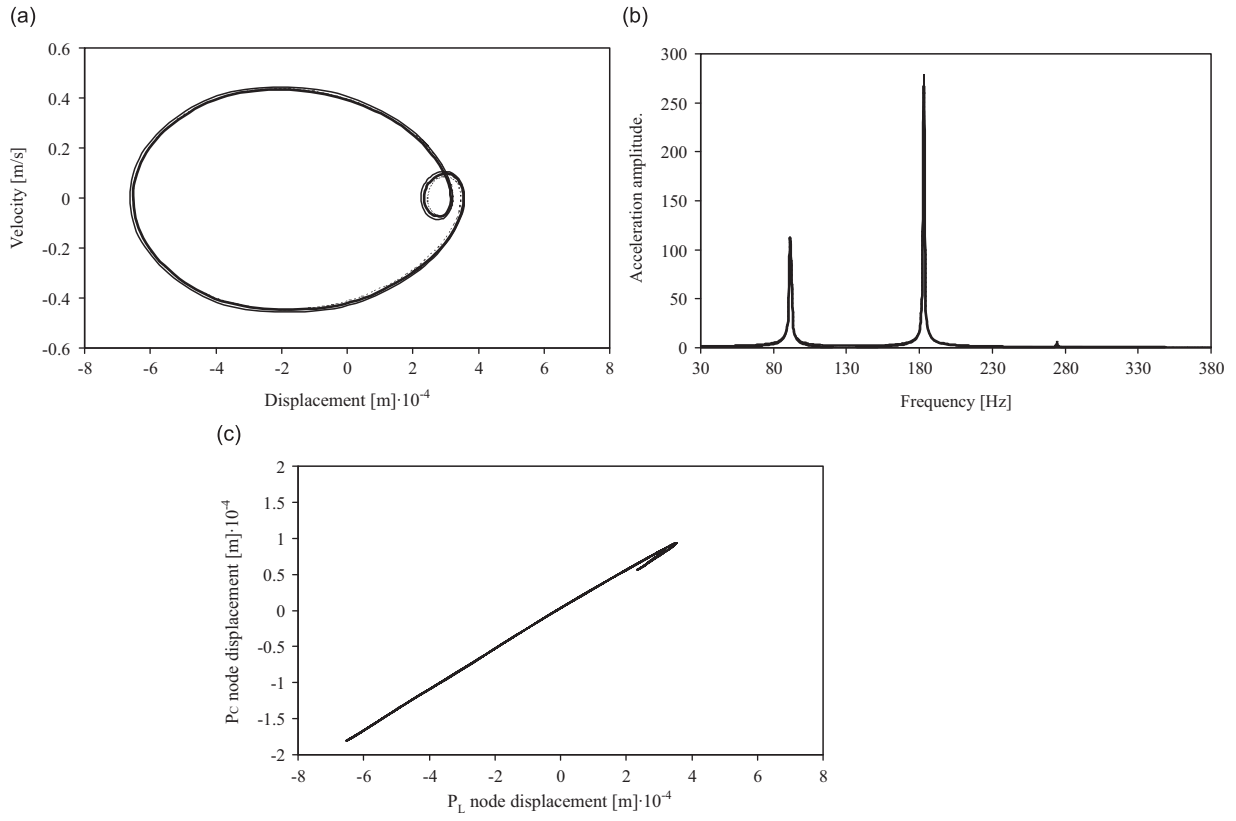

Fig. 10. Case $p=0.47$, $s=0.3$, $\eta=1/2$ (2-D, thick solid line; 1-D, thin solid line; sdof, dashed line): (a) phase portraits, (b) Fourier spectra, and (c) 2-D modal line.

So the quantitative NDIs are as follows:

- the trajectory eccentricity e_d;
- the excursion variation D_v; and
- the harmonic amplitude h_r.

Table 2 reports the values of the damage parameters for each position, severity, and harmonic component for the 2-D model.

As it is clear by their definition, the NDIs values e_d, h_r, and D_v are equal to zero for the undamaged structure; in fact, the orbit is centred in the origin of the phase plane (e_d,=0) and only the fundamental harmonic does exist ($h_r=0$) in the intact beam; as regards D_v, if the beam remains in the undamaged state, the total excursion $D=d_{\max}-d_{\min}$ does not change ($D^{\text{int}}=D^{\text{dam}}$) and hence $D_v=D^{\text{dam}}-D^{\text{int}}$ equals zero. Moreover, the NDIs parameters will grow up with increasing damage level as it is possible to check by the examination of Table 2 and Figs. 14–16.

Indeed it is evident that the values of e_d, D_v and h_r will raise as the severity depth raises from 0.1 to 0.5. For example the h_r value of a beam with a crack positioned at 0.267 of its length and forced with a $\eta=1/2$ harmonic will show an $n=2$ super-harmonic whose normalized magnitude will be equal to 166% for the 0.1 severity, 241% for the 0.3 severity and 417% for the 0.5 severity. In every case it is worthily noted that the absolute value is remarkable, even if the damage is small (i.e. 0.1 severity), confirming the reliability of the damage detection method and the appropriate choice of the quantitative NDIs.

Even if all the harmonic components $n=3, 2, 1/2$ associated to the investigated forcing frequencies $\eta=1/3, 1/2, 2$, exhibit an excellent sensitivity to the damage, they are capable of detecting the damage itself with different efficiencies through the damage parameters of the proposed set $\boldsymbol{\Psi}=\{e_d, D_v, h_r\}$. In order to compare the performances of the above mentioned driving frequencies and response harmonics on the basis of the available numerical results, a special indicator is adopted:

$$I(n,\boldsymbol{\Psi})=\frac{1}{n_p}\sum_{p}\frac{1}{n_s}\sum_{s}\Psi(p,s,n) \tag{14}$$

For brevity's sake, the comparison is limited only to the 2-D model; this indicator is calculated for each one of the harmonic components, and is defined by Eq. (14) as the average value of each one of the damage parameters, calculated over the n_s severities and the n_p positions; Table 3 reports the values which the indicator defined by Eq. (14) assumes for

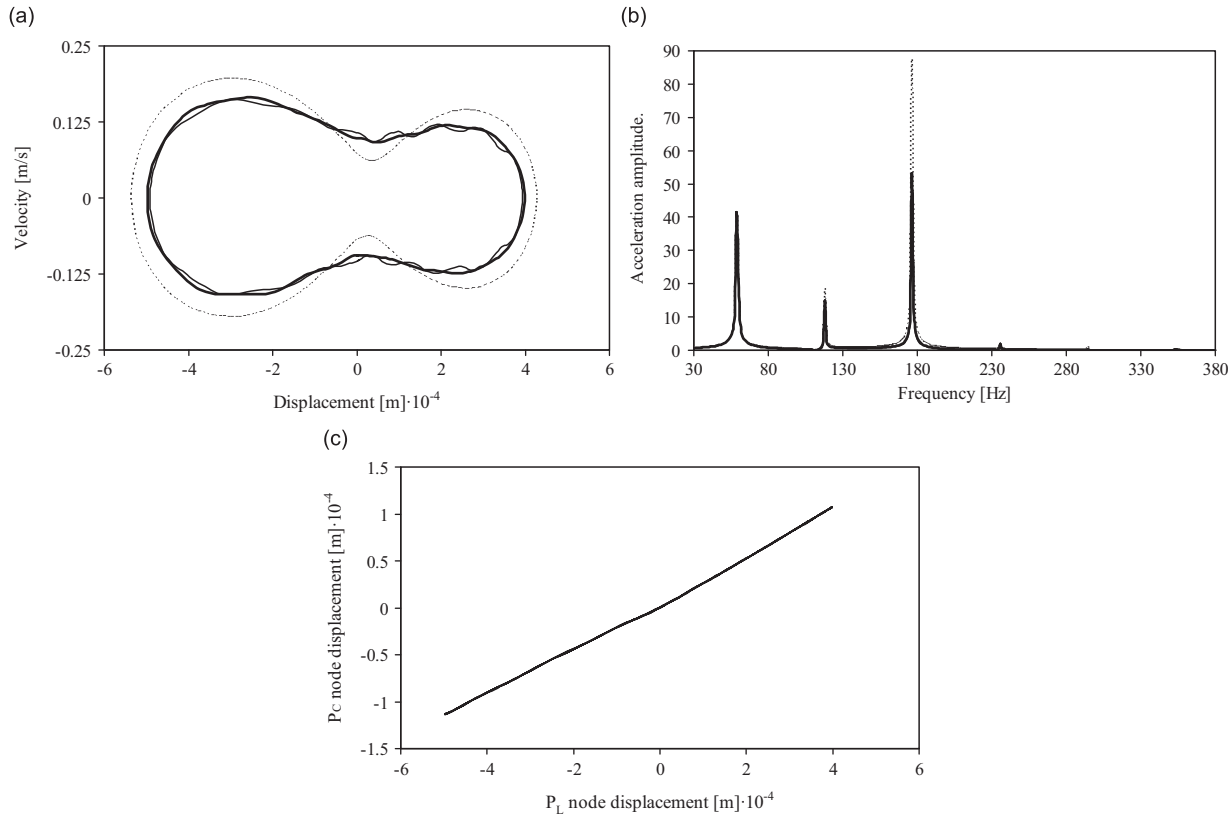

Fig. 11. Case p=0.47, s=0.5, η=1/3 (2-D, thick solid line; 1-D, thin solid line; sdof, dashed line): (a) phase portraits, (b) Fourier spectra, and (c) 2-D modal line.

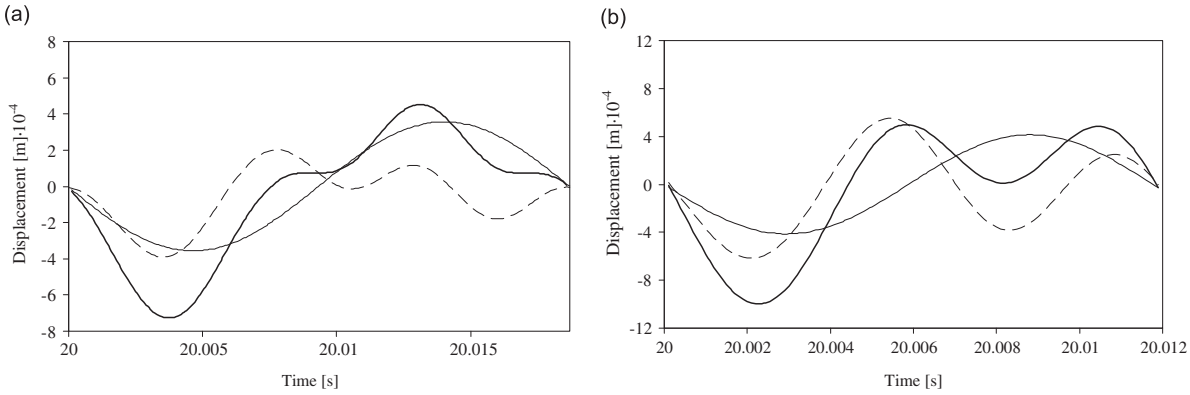

Fig. 12. Decomposition of motion during one driven period of the 2-D model (thick solid line, intact; thin solid line, damaged; dashed line, difference): (a) p=0.08, s=0.5, η=1/3 and (b) p=0.27, s =0.5, η=1/2.

each harmonic component and each damage parameter. Thus, the forcing frequencies η=1/2 and 2 seem the most suitable candidates in order to detect the damage in an efficient way.

So far the whole damage detection procedure can be summarised as follows:

i. estimation of the first natural frequency f_b of the structure via spectral analysis of the free vibration under impulsive loading;
ii. excitation of forced vibration with the most efficient driving frequency η=1/2, i.e. f_F=1/2f_b; and
iii. evaluation of an NDI, e.g. h_r, whose value will detect the damage presence.

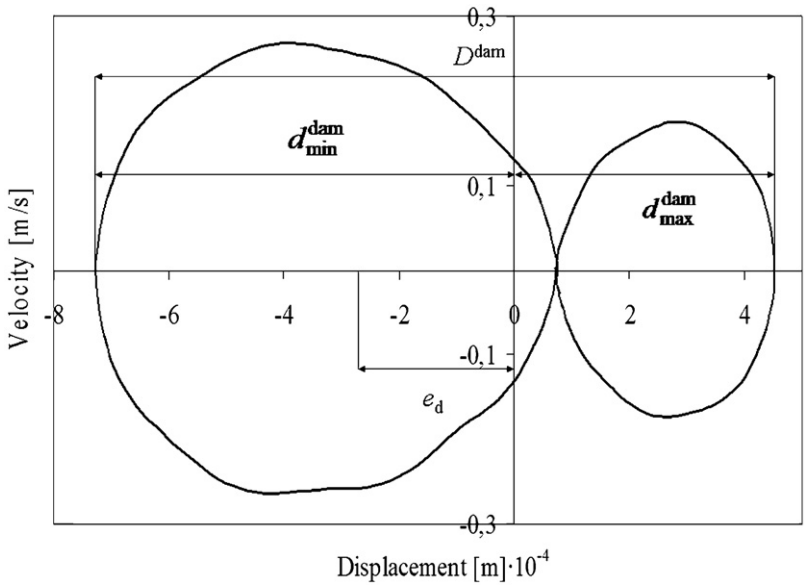

Fig. 13. Graphic illustration of the NDIs meaning.

Table 2
Values of the NDIs for the 2-D model.

Parameter			e_d (μm)	D_v (μm)	h_r (%)
Position	Severity	Harmonic			
0.083	0.1	3	−4.0	8.6	8.0
		2	−140.0	218.0	188.2
		1/2	−53.0	231.8	29
	0.3	3	−40.3	118.1	93.5
		2	−194.3	312.3	311.0
		1/2	−96.2	369.5	221.4
	0.5	3	−136.9	445.2	305.9
		2	−270.4	651.8	439.0
		1/2	−180.7	964.7	585.2
0.267	0.1	3	−2.6	5.1	2.1
		2	−92.0	104.5	166.0
		1/2	−9.1	129.8	9
	0.3	3	−24.2	52.5	30.0
		2	−180.2	225.8	241.0
		1/2	−53.5	156.7	123.0
	0.5	3	−91.2	367.4	287.0
		2	−250.4	632.9	417.0
		1/2	−143.9	718.1	489.0
0.467	0.1	3	−1.3	1.8	1.7
		2	−66.9	85.0	159.0
		1/2	−2	3.2	3
	0.3	3	−12.6	16.6	28.0
		2	−149.1	143	221.0
		1/2	−11	24	5
	0.5	3	−49.7	162.5	130.0
		2	−223.9	550.9	384.0
		1/2	−31.4	92.2	83.0

The NDI h_r is selected because it can be easily evaluated via spectral analysis of acceleration measurements made online by means of simple devices like mass accelerometer, connected to the beam tip.

The numerical results discussed in Section 3 were obtained by harmonically forcing a beam model where crack positions and lengths were fixed *a priori*; however, the quantitative NDIs herein defined can nevertheless be evaluated also when only the numerical and/or experimental responses are known, without performing the analyses or the responses

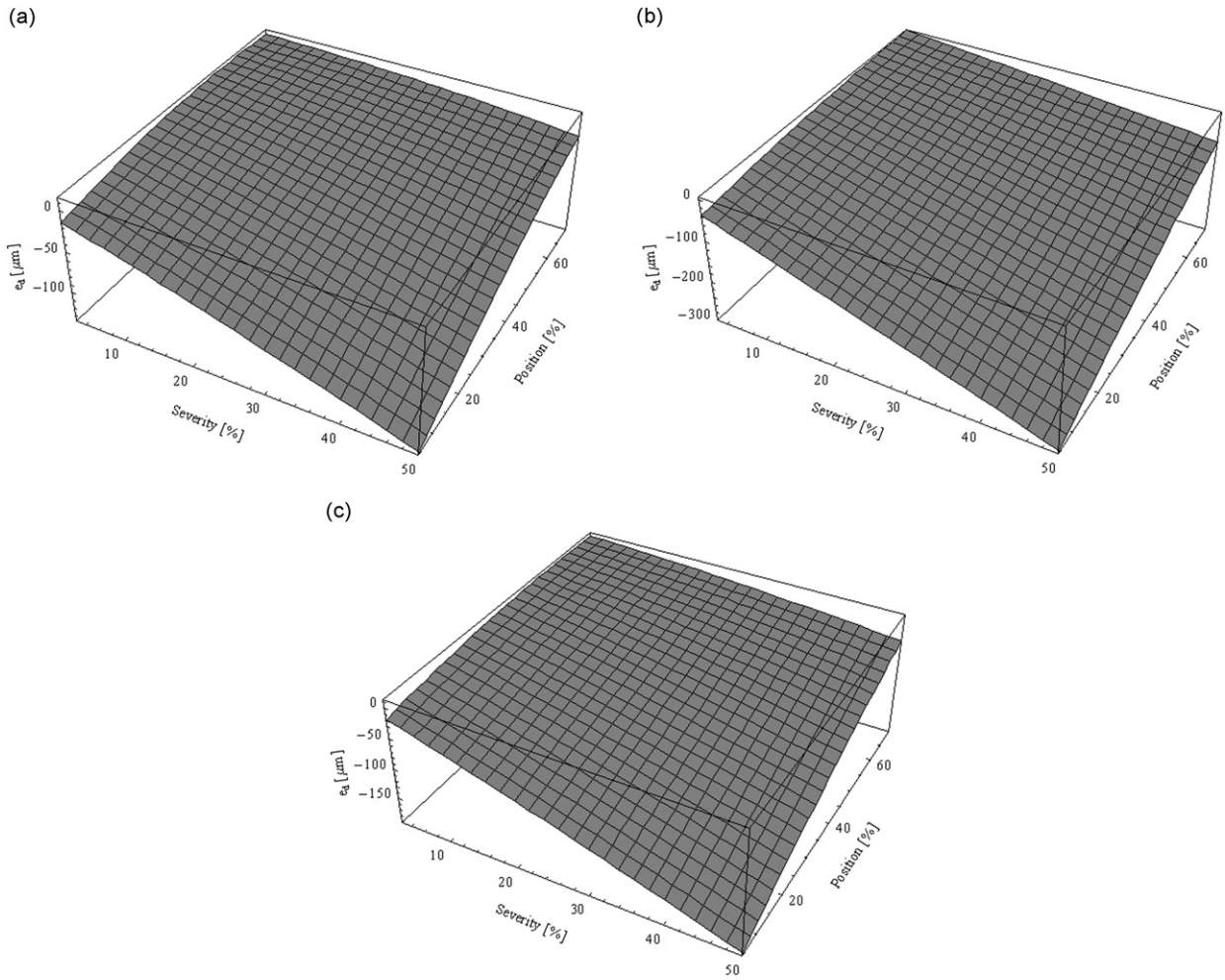

Fig. 14. Eccentricity e_d with respect to the origin in the phase portraits: (a) super-harmonic component 3, (b) super-harmonic component 2, and (c) sub-harmonic component 1/2.

having be independently provided. Thus, the crucial question "Is this structure intact or damaged?" can be easily answered and the damage status of the structure assessed in any case by (i) using an accelerometer, (ii) measuring tip accelerations, (iii) analysing the frequency content, and (iv) evaluating a simple damage indicator, provided that geometry and material of the structure be known.

5. Construction of the calibration surfaces

Once the values of the damage parameters e_d, D_v, and h_r have been calculated (Table 2) for each one of the three positions, severities, and harmonic components *a priori* fixed, calibration surfaces are constructed by interpolating the damage indicators (DII).

In more details, least-squares fit to the values of the damage parameters $\mathbf{\Psi}=\{e_d, D_v, h_r\}$ reported in Table 2 for each one of the harmonic components $n=\left\{3 \quad 2 \quad 1/2\right\}$ in the position-severity plane p–s generates quadratic surfaces of the form

$$\Psi_n = a_{n,\Psi}p^2 + b_{n,\Psi}ps + c_{n,\Psi}s^2 + d_{n,\Psi}p + e_{n,\Psi}s + f_{n,\Psi} \tag{15}$$

at the left hand side there is the level Ψ_n, of the damage parameter belonging to the set $\mathbf{\Psi}$ and corresponding to the nth harmonic component; the numerical coefficients of Eq. (15) depend on both the number "n" of the harmonic component and the type of the damage parameter, e.g. $a=\hat{a}(n,\Psi)$. The values of the coefficients of Eq. (15) are reported in Table 4.

In this way it is possible to generate the damage surfaces depicted in the three-dimensional Figs. 14–16. Such surfaces numerically interpolate the calculated results and graphically represent the damage measures e_d, D_v, and h_r as functions of the two spatial variables which geometrically characterize the crack, namely position p and severity s. In more detail, each

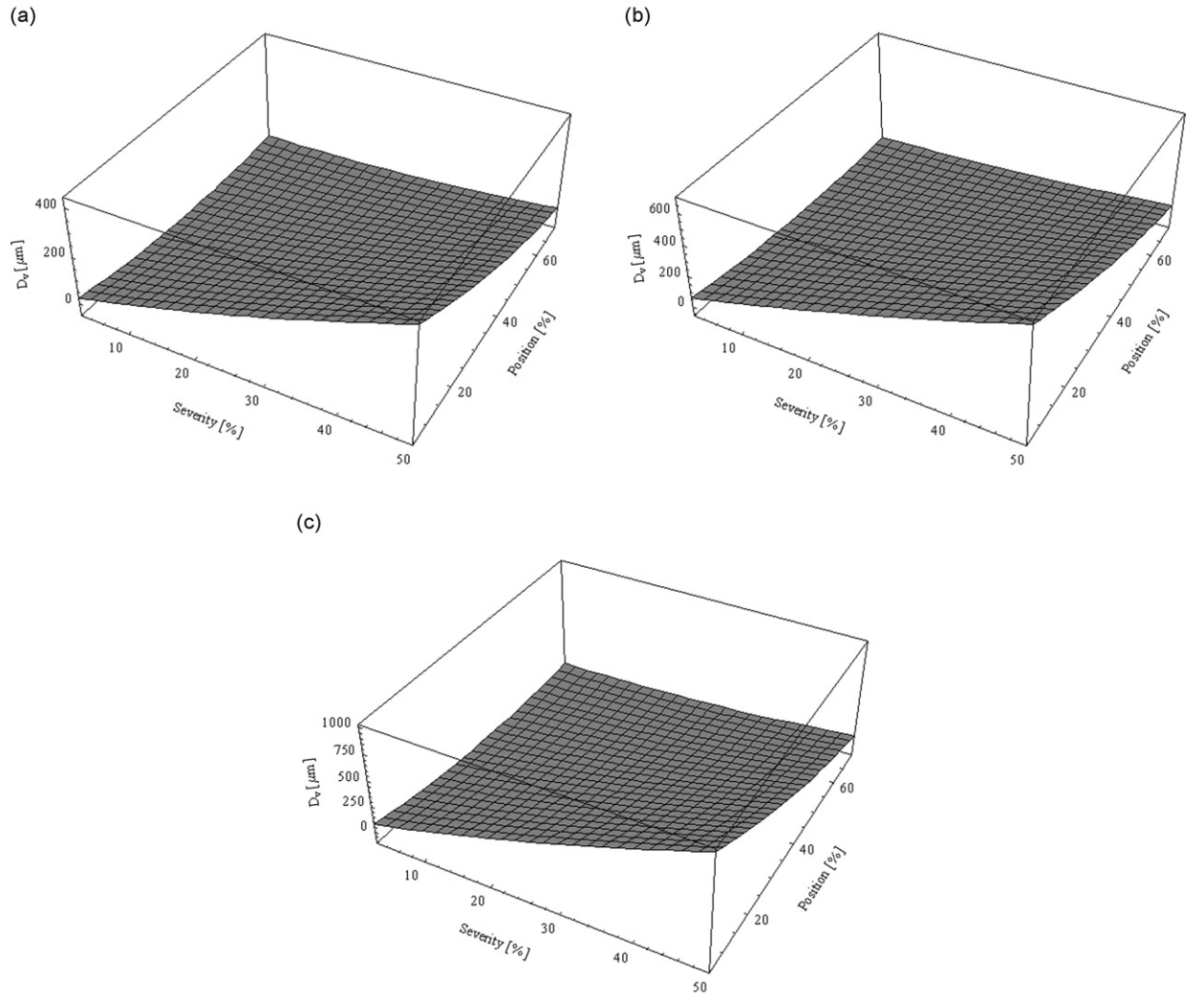

Fig. 15. Variation D_v of the total excursion in the phase portraits: (a) super-harmonic component 3, (b) super-harmonic component 2, and (c) sub-harmonic component 1/2.

figure illustrates the dependence of the relevant damage measure on the harmonic component at hand, namely super-harmonic $n=3$ in Figs. 14a–16a, super-harmonic $n=2$ in Figs. 14b–16b, and sub-harmonic $n=1/2$ in Figs. 14c–16c.

As it has already said, the general trends exhibited in Figs. 14–16 are not surprising, inasmuch the values of the damage measures tend to decrease with the distance from the cantilever root and with the vanishing of the crack length. It is now possible to relate the orbit eccentricity (Fig. 14), excursion variation (Fig. 15), and harmonic amplitude (Fig. 16) not only to the presence of damage (i.e. non-zero values of NDIs), but also to the position and even to the size of it.

6. Identification of the damage

Suppose now to know only the numerical and/or experimental responses of the presumably cracked beam: once the damage status of the structure has been assessed, the next goal is to solve the inverse problem, i.e. to evaluate the unknown position and depth of the defect, generally different of those used to construct the calibration surfaces. In the following a procedure of crack location and size estimation is proposed which is based on using preliminary constructed calibration surfaces (DII) of Section 5. So far, a procedure for damage identification may be designed according to the following steps:

i. evaluate the bilinear frequency of the damaged system by spectral analysis of the acceleration time-history recorded at the beam tip due to an impulsive force;

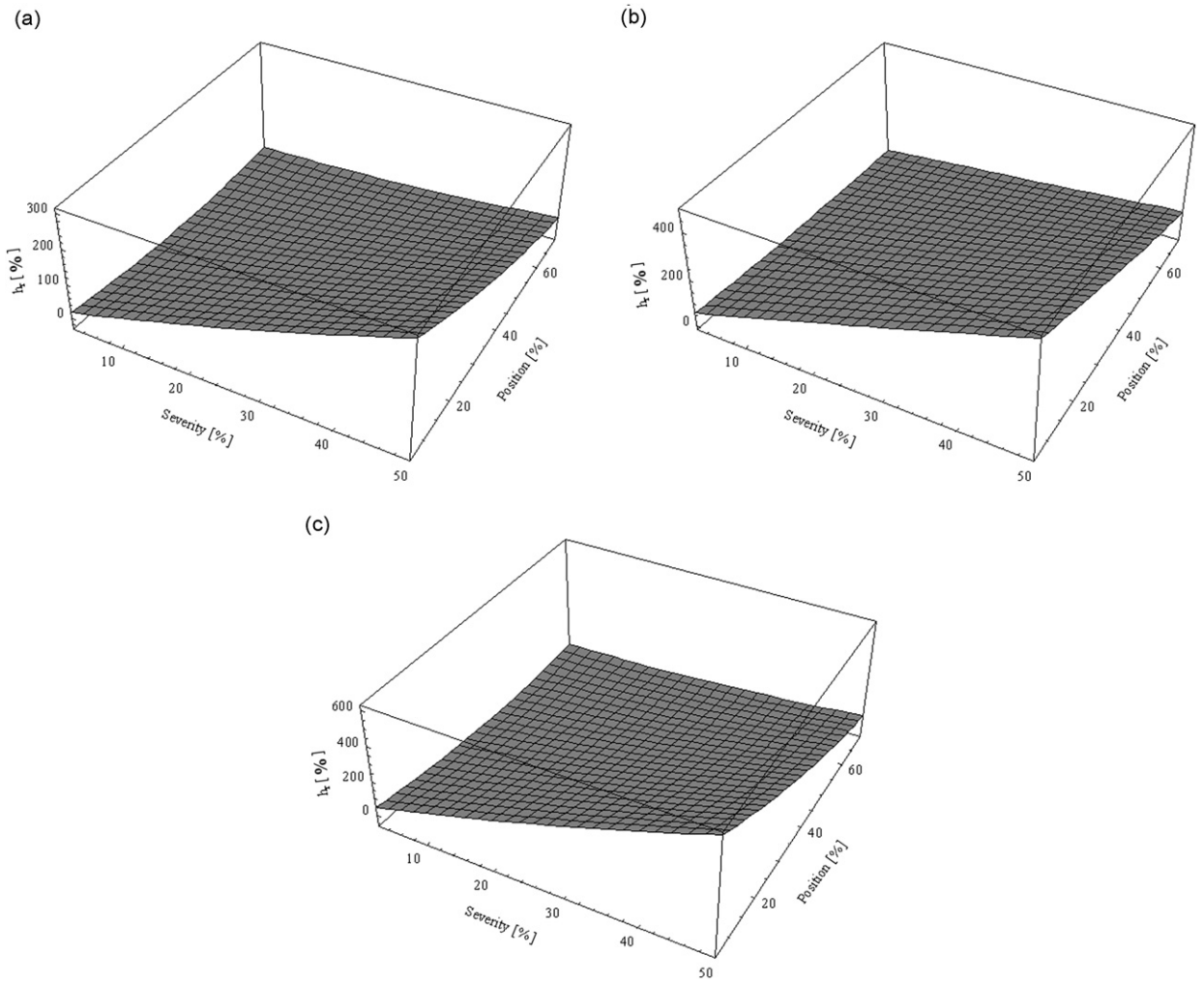

Fig. 16. Relative amplitude h_r in the Fourier spectra: (a) super-harmonic component 3, (b) super-harmonic component 2, and (c) sub-harmonic component 1/2.

Table 3
Efficiency of driving frequencies to detect damage.

Damage parameter	e_d (μm)	D_v (μm)	h_r (%)
Frequency $\eta=f_F/f_b$			
1/3	−40.3	130.9	98.5
1/2	−174.1	324.9	280.7
2	−64.5	298.9	172

ii. excite the structure with a driving force having frequencies equal to, respectively, one half and twice the bilinear frequency of the system, which was estimated in the previous step; the values $\eta=1/2$, 2 are selected because of their better performances in damage detection, as it has been demonstrated in the previous Section 4;
iii. choice and evaluate the NDI h_r; and
iv. solve the following system of two algebraic nonlinear equations:

$$\begin{cases} a_{h,2}p^2+b_{h,2}ps+c_{h,2}s^2+d_{h,2}p+e_{h,2}s+f_{h,2}=h_{r,2} \\ a_{h,1/2}p^2+b_{h,1/2}ps+c_{h,1/2}s^2+d_{h,1/2}p+e_{h,1/2}s+f_{h,1/2}=h_{r,1/2} \end{cases} \Rightarrow (\tilde{p},\tilde{s}) \tag{16}$$

the subscripts of the coefficients in Eq. (16) identify, respectively, the type (h stands for "relative amplitude of the harmonic component with respect to the fundamental one", Eq. (13)) and the order of the harmonic component itself (n=2, 1/2) affecting the damage parameter; the known terms at the right hand side are the values of the damage

Table 4
Coefficients of the quadrics Eq. (9).

Damage parameter	Harmonic component	a	b	c	d	e	f
e_d (μm)	3	−0.01396	0.03181	−0.01017	1.31129	−2.07608	−10.54260
	2	−0.00797	0.05908	−0.00305	1.04937	−5.49759	−28.38590
	1/2	−0.00989	0.04297	−0.00865	0.99393	−3.34188	−14.45560
D_v (μm)	3	0.06719	−0.14629	0.07812	−5.44546	6.29874	12.11200
	2	0.04425	−0.16022	0.03668	−4.36159	11.98280	51.86510
	1/2	0.11592	−0.29029	0.13940	−9.52081	14.07510	38.64150
h_r (%)	3	0.03517	−0.08179	0.03986	−2.91915	3.92146	11.10210
	2	0.01225	−0.09900	0.00585	−1.65809	9.14444	45.26370
	1/2	0.05558	−0.15926	0.05803	−4.93372	9.64383	37.28650

parameters calculated via numerical simulations and/or measured via experimental tests, in different cases with respect to those used to generate the coefficients of Eqs. (16). The solution of the system equations (16) gives an estimation of both position and severity ($\check{p}$,$\check{s}$) of the crack.

v. evaluate the confidence of the solution.

The confidence of such an approximate evaluation can be calculated by using the remaining two damage parameters e_d and D_v, the measure of which needs more sophisticated test instruments like Laser vibrometers and/or numerical integration of acceleration time-histories:

$$\begin{cases} a_{e,2}p^2+b_{e,2}ps+c_{e,2}s^2+d_{e,2}p+e_{e,2}s+f_{e,2}=e_{d,2} \\ a_{e,1/2}p^2+b_{e,1/2}ps+c_{e,1/2}s^2+d_{e,1/2}p+e_{e,1/2}s+f_{e,1/2}=e_{d,1/2} \end{cases} \Rightarrow (\check{p},\check{s}) \tag{17}$$

$$\begin{cases} a_{D,2}p^2+b_{D,2}ps+c_{D,2}s^2+d_{D,2}p+e_{D,2}s+f_{D,2}=D_{v,2} \\ a_{D,1/2}p^2+b_{D,1/2}ps+c_{D,1/2}s^2+d_{D,1/2}p+e_{D,1/2}s+f_{D,1/2}=D_{v,1/2} \end{cases} \Rightarrow (\widehat{p},\widehat{s}) \tag{18}$$

The first subscript of the coefficients of Eqs. (17) and (18) denotes the number of the harmonic components (n=2, 1/2), whereas the second subscript indicates the type of damage parameter: e for "eccentrity", Eq. (11), and D for "excursion", Eq. (12); the known terms at the right hand side are the values of the damage parameters calculated via numerical simulations and/or measured via experimental tests in different cases with respect to those used to generate the coefficients of Eqs. (16)–(18). These further estimations ($\check{p}$,$\check{s}$) and $\left(\widehat{p},\widehat{s}\right)$ of position and severity of the crack can provide a measure of the reliability of the damage identification.

Each one of the second-order systems of Eqs. (16)–(18) generally has four solutions in the unknowns p and s; in the problem at hand two solutions were complex conjugate and the other two real ones; in most cases only one of these real solutions was physically or technically meaningful; in other cases the two real solutions allowed the strict confining of the ranges where crack position and severity could be identified. For sample's sake, two cases of practical interest were examined in major detail. In the first case, the actual values p=10% and s=40% of position and severity of the crack were detected (Section 4) by numerically or experimentally measuring $h_{r,2}$=365.1% and $h_{r,1/2}$=381.8%, $e_{d,2}$=256.1 μm, $e_{d,1/2}$=125.8 μm, $D_{v,2}$=439.3 μm, and $D_{v,1/2}$=617.3 μm. Then, the identification procedure of Section 6 yielded two real solutions, the first of which was

system (16)$\rightarrow p\cong 9\%$, $s\cong 39\%$,
system (17)$\rightarrow p\cong 12\%$, $s\cong 41\%$, and
system (18)$\rightarrow p\cong 7\%$, $s\cong 37\%$.

A simple statistical processing led to confidence intervals (95%) of $p=9.3\pm 2.3\%$ and $s=39\pm 1.8\%$.
The second solution was

system (16)$\rightarrow p\cong 60\%$, $s\cong 92\%$,
system (17)$\rightarrow p\cong 59\%$, $s\cong 94\%$, and
system (18)$\rightarrow p\cong 56\%$, $s\cong 88\%$.

Thus, confidence intervals (95%) were $p=58.3\pm 1.9\%$ and $s=91.3\pm 2.8\%$. It is evident that only the first solution is technically acceptable because it lays below a reasonable upper limit of crack severity, beyond which the beam falls dramatically apart. It is worth to be noted that the actual damage p=10% and s=40% is comprised within the confidence interval $9.3-2.3<p<9.3+2.3$ and $39-1.8<s<39+1.8$.

As a further example, the actual damage characterized by position p=40% and severity s=5% was detected (Section 4) by numerically or experimentally measuring $h_{r,2}$=41.7% and $h_{r,1/2}$=79.2%, $e_{d,2}$=44.5 μm, $e_{d,1/2}$=13.1 μm, $D_{v,2}$=13.8 μm,

and $D_{v,1/2}$=173.6 μm. Then, the identification procedure of Section 6 yielded two real solutions, the first of which was

system (16)→$p \cong 56\%$, $s \cong 8\%$,
system (17)→$p \cong 54\%$, $s \cong 9\%$, and
system (18)→$p \cong 52\%$, $s \cong 8\%$.

Thus, confidence intervals (95%) were $p=54 \pm 1.8\%$ and $s=8.3 \pm 0.5\%$.
The second solution was

system (16)→$p \cong 39\%$, $s \cong 5\%$,
system (17)→$p \cong 38\%$, $s \cong 4.5\%$, and
system (18)→$p \cong 38\%$, $s \cong 4.5\%$.

Thus, confidence intervals (95%) were $p=38.3 \pm 0.5\%$ and $s=4.7 \pm 0.3\%$.

In this case, there were two real and acceptable solutions, but they were confined within a restricted range of values $38.3–0.5 < p < 54+1.8$, $4.7–0.3 < s < 8.3+0.5$.

It is worth noting that the first case represented severe damage inasmuch the crack was near the built-in end of the beam and almost half of the cross-section high; in the second case, the crack had small size and was far from the built-in end, a configuration usually difficult to be detected. In any case, the narrow ranges of identified position and severity allowed to limit the observation field. Furthermore, it was observed that the actual damage was comprised within the confidence intervals and hence considering solutions of systems (17) and (18) beside that of system (16) allowed an improvement of the confidence of the damage estimation.

At the end, the complete question "Is this structure intact or damaged and, if it is damaged, how much are the damage position and size?" has been actually answered by the above described procedure of identification. A cracked structure can be detected and identified by a common accelerometer, simple measurements and easy numerical computations.

Of course, if the geometry and material assumptions on which this method is based are not satisfied, the approximation of the defect position and severity could not pick the real values with sufficient accuracy. For instance, the given assumption of non-propagating crack running through the whole width of the beam is often encountered in engineering practice and widely adopted in Literature. If it was non-satisfied, the values of the NDIs and especially D_v and e_d could not match at the desired extent with the coefficients of the quadratic equation corresponding to crack not running through the whole width.

7. Comparison among structural models

It is worthily noted that the three structural models of Sections 2.2, 2.4, and 2.5 provided results which are in good agreement with each other whatever the representation used (phase portrait, Fourier spectrum, modal line), as demonstrated in Section 3.2 and showed in Figs. 6–11. Indeed the three models exhibited the same qualitative dynamic behaviour and the previous considerations, analyses and procedures, which have been developed with reference to the 2-D solid model for synthesis'sake, may be implemented by using the 1-D beam and sdof oscillator models as well.

Thus, it seemed not useless to compare the performances of these simpler structural models with respect to the results provided by 2-D one, assumed as reference model; obviously, the analyses conducted by means of the 1-D beam and the bilinear sdof oscillator models needed much less computational requirements in terms of time consuming and memory occupying than those worked out by using the 2-D FEM solid model. While it was already observed that all the three models are in very good agreement with each other from the qualitative point of view, a quantitative estimation of their reliability is sought: a special indicator has been adopted which allows to evaluate the relative differences affecting the behaviours of the simpler models with respect to the more demanding 2-D model. For each one of the two models of the subset M={1-D FEM, sdof}, this indicator is defined as the average value calculated over the n_Ψ Nonlinear Damage Indicators, the n_h harmonics, the n_s severities, and the n_p positions:

$$J(M,p,s,n,\boldsymbol{\Psi}) = \frac{1}{n_p}\sum_p \frac{1}{n_s}\sum_s \frac{1}{n_h}\sum_h \frac{1}{n_\Psi}\sum_\Psi \frac{\Psi(M,p,s,n)-\Psi(2D,p,s,n)}{\Psi(2D,p,s,n)} \tag{19}$$

Table 5
Comparison among the structural models.

J	e_d (%)	D_v(%)	h_r(%)	Average offset (%)
1-D vs. 2-D	6	20	19	16
sdof vs. 2-D	10	41	27	27

Thus, Eq. (19) yields one value of the indicator for each one of the two models 1-D FEM e sdof: $J(\text{1-D}) \cong 16\%$ and $J(\text{sdof}) \cong 27\%$, which show that the 1-D FEM beam performs better than the sdof oscillator, as it could be expected. Furthermore, the 1-D FEM beam is able to catch with sufficient accuracy also the quantitative aspects of the 2-D FEM solid, even by using a very limited number of beam elements, whereas the bilinear sdof model overestimate at some extent the response of the 2-D solid model, due to the influence of the upper modes of vibration of the continuous beam.

The values of the indicator J are reported in Table 5 for 1-D and sdof models as well as the average differences between the models for every NDI.

8. Conclusion

Many of the researchers in the cited Literature assumed in their work that the crack in a structural element is open and remains open during vibration. This assumption was made to avoid the uncomfortable drawbacks arising from the nonlinear characteristics presented by introducing a breathing crack. It is evident that using an open-crack model assumption to interpret vibration measurements for a fatigue-breathing crack will lead to the incorrect conclusion that the crack severity is smaller than what it really is.

It was shown both numerically and experimentally that the appearance of a fatigue crack has a stimulating influence on the appearance of a new set of nonlinear properties, which do not occur in the initially undamaged structure (self-excitation of sub-harmonic regimes, appearance of even- and odd-numbered harmonic components in frequency spectrum of $n/1$-order super-harmonic regime). In particular, the characteristics of nonlinear distortion of vibrations at super-harmonic resonance of the beam of order 3/1 and 2/1 (i.e. third and second harmonics) are very sensitive to the presence of closing crack; moreover, the appearance of nonlinear effects when the structure is harmonically excited at a frequency, which is a sub-multiple of a natural frequency, can be used to detect the presence of very small closing cracks.

This paper presents an analysis of bending harmonic forced vibrations of a cantilevered beam with a transverse one-edge non-propagating closing crack. In the methods observed in the Literature compromises have been made either in the representation of the physics of the nonlinearities in defective structures or in the complexity of the structure which can be analysed. For example, finite element studies usually use a simplistic representation of the interface mechanics whereas analytical studies require simple boundary conditions. Herein, the simulation of the harmonic forced vibrations of the beam, a nonlinear finite element procedure has been developed with (a) two-dimensional solid model, (b) one-dimensional beam model, and (c) single-degree-of-freedom system model. The two-dimensional model, though expensive, can be used to simulate the nonlinear interface effects of partial depth breathing crack as a contact problem under dynamic conditions. Furthermore qualitative and quantitative comparisons among the different models were illustrated in the paper.

In the present work, it was observed that even for a small crack, if the excitation frequency was approximately one-third, one-half, and two times of the first natural frequency of the system, the relative amplitude of the third, second, and one-half harmonics respectively became appreciably large and hence detectable. The description of these nonlinear dynamic behaviours was synthetized by the definition of qualitative Nonlinear Damage Indicators (NDIs): the phase portrait distortions, the super- and sub-harmonic resonances in the FFT spectra, the curved shape trend of the modal lines. In order to improve the application of these indicators for the damage detection, three quantitative NDIs were proposed as well: the orbit eccentricity e_d, the excursion variation D_v, the harmonic amplitude h_r.

Using these NDIs allowed to develop a new and highly sensitive vibration-based procedure for crack detection by analysing super- and sub-harmonic components in the force response of a beam, which originated from a breathing crack. It was shown that the detection sensitivity of the proposed nonlinear method was much higher than that one obtainable from usual linear vibration procedures. Both super- and sub-harmonics components were in fact efficient indicators of the crack presence and were used to improve the accuracy of vibration-based crack detection techniques. Moreover, a systematic and complete identification procedure was developed to evaluate both the crack presence and the crack position and depth. The core of this method was the Damage Indicators Interpolation (DII), the implementation of which allowed to construct surfaces that related the crack position and depth to each one of the NDI value.

The proposed procedure, which required the driving force to be applied at the beam tip and the sensor to have only one location, allowed to detect the presence of the crack and was used to estimate the crack parameters, i.e. to determine both crack size and location. Only acceleration time-history was needed to detect the existence of the crack as well as to establish the relationship between the nonlinear characteristics of the response with the crack depth; moreover, only few measurements were needed to estimate the crack site. Furthermore, the use of acceleration signal facilitated remote monitoring of the structure for fatigue cracks when the crack site was unknown. The numerical simulations worked out in this study for samples'sake demonstrated that the proposed method was applied to detect small cracks with the lengths of few percentual units of the cross-section.

Acknowledgements

This research was partially funded by "Progetto di Ateneo 2006" under Grant no. C26A059503 and "Progetto di Università" under Grant no. C26A07TELB of "Sapienza" University of Rome. The authors want to gratefully acknowledge Dr. Luca Placidi for his contribution in generating the damage interpolation surfaces.

References

[1] M. Chati, R. Rand, S.J. Mukherjee, Modal analysis of a cracked beam, *Journal of Sound and Vibration* 207 (1997) 249–270.
[2] M.H.H. Shen, Y.C. Chu, Vibrations of beams with a fatigue crack, *Computers and Structures* 45 (1) (1992) 79–93.
[3] E. Douka, L.J. Hadjileontiadisb, Time–frequency analysis of the free vibration response of a beam with a breathing crack., *Independent Nondestructive Testing and Evaluation International* 38 (2005) 3–10.
[4] Z.Q. Lang, Z.K. Peng, A novel approach for nonlinearity detection in vibrating systems, *Journal of Sound and Vibration* 314 (3–5) (2008) 603–615.
[5] S.J. Chinchalkar, Determination of crack location in beams using natural frequencies, *Journal of Sound and Vibration* 247 (2001) 417–429.
[6] S.D. Panteliou, T.G. Chondros, V.C. Argyrakis, A.D. Dimarogonas, Damping factor as an indicator of crack severity, *Journal of Sound and Vibration* 241 (2001) 235–245.
[7] J.T. Kim, Y.S. Ryu, H.M. Cho, N. Stubbs, Damage identification in beam-type structures: frequency-based method vs. mode-shape-based method, Engineering Structures 25 (2003) 57–67.
[8] A.P. Bovsunovsky, C. Surace, Considerations regarding superharmonic vibrations of a cracked beam and the variation in damping caused by the presence of the crack, *Journal of Sound and Vibration* 288 (2005) 865–886.
[9] V.K. Nguyen, O.A. Olatunbosun, A proposed method for fatigue crack detection and monitoring using the breathing crack phenomenon and wavelet analysis, *Journal of Mechanics of Materials and Structures* 2 (3) (2007) 399–420.
[10] T.G. Chondros, A.D. Dimaragonas, Y.J. Yao, Vibration of a beam with a breathing crack, *Journal of Sound and Vibration* 239 (2001) 57–67.
[11] U. Andreaus, P. Baragatti, Fatigue crack growth, free-vibrations and breathing crack detection of aluminium alloy and steel beams, *Journal of Strain Analysis for Engineering Design* 44 (7) (2009) 595–608.
[12] S. Benfratello, P. Cacciola, N. Impollonia, A. Masnata, G. Muscolino, Numerical and experimental verification of a technique for locating a fatigue crack on beams vibrating under Gaussian excitation, *Engineering Fracture Mechanics* 74 (2007) 2992–3001.
[13] Y.C. Chu, M.H.H. Shen, Analysis of forced bilinear oscillators and the application to cracked beam dynamics, *Journal of American Institute of Aeronautics and Astronautics* 30 (10) (1992) 2512–2519.
[14] J.N. Sundermeyer, R.L. Weaver, On crack identification and characterization in a beam by nonlinear vibration analysis, *Journal of Sound and Vibration* 183 (1995) 857–871.
[15] O.N.L. Abraham, J.A. Brandon, The modelling of the opening and closing of a crack, *Journal of Vibration, Acoustics, Stress and Reliability in Design—Transactions of the ASME* 117 (1995) 370–377.
[16] M. Kisa, J. Brandon, The effects of closure of cracks on the dynamics of a cracked cantilever beam, *Journal of Sound and Vibration* 238 (1) (2000) 1–18.
[17] N. Pugno, C. Surace, R. Ruotolo, Evaluation of the nonlinear dynamic response to harmonic excitation of a beam with several breathing cracks, *Journal of Sound and Vibration* 235 (5) (2000) 749–762.
[18] K. Kamiya, T. Yoshinaga, Nonlinear steady-state vibration analysis of a beam with breathing cracks (finite element analysis based on the mixed variational principle), *Journal of System Design and Dynamics* 2 (3) (2008) 750–761.
[19] P.N. Saavedra, L.A. Cuitino, Crack detection and vibration behavior of cracked beams, *Computers and Structures* 79 (2001) 1451–1459.
[20] A. Nandi, S. Neogy, Modelling of a beam with a breathing edge crack and some observations for crack detection, *Journal of Vibration and Control* 8 (5) (2002) 673–693.
[21] S.L. Tsyfansky, V.I. Beresnevich, Detection of fatigue cracks in flexible geometrically nonlinear bars by vibration monitoring, *Journal of Sound and Vibration* 213 (1998) 159–168.
[22] S.L. Tsyfansky, V.I. Beresnevich, Nonlinear vibration method for detection of fatigue cracks in aircraft wings, *Journal of Sound and Vibration* 236 (1) (2000) 49–60.
[23] V.V. Matveev, A.P. Bovsunvsky, Vibration-based diagnostics of fatigue damage of beam-like structures, *Journal of Sound and Vibration* 249 (1) (2002) 23–40.
[24] A.P. Bovsunovsky, O. Bovsunovsky, Crack detection in beams by means of the driving force parameters variation at nonlinear resonance vibrations, *Key Engineering Materials* 347 (2007) 413–420.
[25] P.F. Rizos, N. Aspragathos, A.D. Dimarogonas, Identification of crack location and magnitude in a cantilever beam from the vibration modes, *Journal of Sound and Vibration* 138 (3) (1990) 381–388.
[26] T.Y. Kam, T.Y. Lee, Detection of cracks in structures using modal test data, *Engineering Fracture Mechanics* 42 (2) (1992) 381–387.
[27] G.L. Qian, S.N. Gu, J.S. Jiang, The dynamic behaviour and cracked detection of a beam with a crack, *Journal of Sound and Vibration* 138 (2) (1990) 233–243.
[28] S. Christides, A.D.S. Barr, One-dimensional theory of cracked Bernoulli–Euler beams, *International Journal of Mechanic Science* 26 (11–12) (1983) 639–648.
[29] T.G. Chondros, A.D. Dimaronogas, Vibration of a cracked cantilever beam, *Transactions of the American Society of Mechanical Engineers* 120 (1998) 742–746.
[30] P. Gudmundson, The dynamic behaviour of slender structures with cross-sectional cracks, *Journal of the Mechanics and Physics of Solids* 31 (4) (1983) 329–345.
[31] C.A. Papadopolous, A.D. Dimaronogas, Coupled longitudinal and bending vibrations of a rotating shaft with an open crack, *Journal of Sound and Vibration* 117 (1) (1987) 81–93.
[32] J.K. Sinha, M.I. Friswell, S. Edwards, Simplified models for the location of cracks in beam structures using measured vibration data, *Journal of Sound and Vibration* 251 (2002) 13–38.
[33] H. Tada, P.C. Paris, G.M. Irwin, *The Stress Analysis of Cracks Handbook*, Press of American Society of Mechanical Engineers, New York, 2000.
[34] G. Gounaris, A.D. Dimarogonas, A finite element of a cracked prismatic beam for structural analysis, *Computers and Structures* 28 (3) (1988) 309–313.
[35] R. Ruotolo, C. Surace, P. Crespo, D. Storer, Harmonic analysis of the vibration of a cantilevered beam with closing crack, *Computers and Structures* 61 (1996) 1057–1074.
[36] B. Zastrau, Vibrations of cracked structures, *Archives of Mechanics* 37 (1985) 731–743.
[37] F. Ibrahim, A. Ismail, H.R. Martin, Modelling of the dynamics of a continuous beam including nonlinear fatigue crack, *International Journal of Analytical and Experimental Modal Analysis* 2 (2) (1987) 76–82.
[38] M.I. Friswell, J.E.T. Penny, A simple nonlinear model of a cracked beam, *Proceedings of the 10th International Modal Analysis Conference*, San Diego, California, 1992, pp. 516–521.
[39] A. Rivola, P.R. White, Bispectral analysis of the bilinear oscillator with application to the detection of fatigue cracks, *Journal of Sound and Vibration* 216 (5) (1998) 889–910.
[40] A.D. Dimaronogas, C.A. Papadopolous, Vibration of cracked shafts in bending, *Journal of Sound and Vibration* 91 (4) (1983) 583–593.
[41] K.J. Bathe, *Finite Elements Procedure*, Prentice-Hall, Upper Saddle River, New Jersey, 1996.
[42] U. Andreaus, P. Casini, F. Vestroni, Frequency reduction in elastic beams due to a stable crack: numerical results compared with measured test data, *Engineering Transactions* 51 (1) (2003) 1–16.
[43] A. Signorini, *Mathematical Physics*, E.V. Veschi, Rome, Italy, 1951 (in Italian).
[44] W.M. Ostachowicz, M. Krawczuk, Analysis of the effect of cracks on the natural frequencies of a cantilever beam, *Journal of Sound and Vibration* 150 (2) (1991) 191–201.
[45] U. Andreaus, P. Casini, F. Vestroni, Nonlinear dynamics of a cracked cantilever beam under harmonic excitation, *International Journal of Nonlinear Mechanics* 42 (3) (2007) 566–575.